$CD8^+$ T Cell Exhaustion and Immune Checkpoint Inhibitors in Mutant Isocitrate Dehydrogenase I Gliomas

Ali Dabaja

April 22nd, 2022

This thesis has been read and approved by Dr. Maria Castro

Signed:  Date: 04/22/2022

Faculty advisor email: mariacas@umich.edu Phone: 734-764-0850

Table of Contents

Acknowledgments

Scientific Acknowledgments

I would like to sincerely thank the entire Castro-Lowenstein Lab for the support and opportunity they provided me in conducting research in this lab since I have been a sophomore at the university. I would especially like to thank my mentor Brandon McClellan and working alongside Rohit Thalla, who have helped me throughout the entire process, allowing me to grow my laboratory skills and techniques throughout my time as an undergrad. It has been a privilege working and learning alongside everyone in the lab and hope to continue doing so while moving forward with my education.

Personal Acknowledgments

I would like to thank my friends and family who have supported me while working on writing my thesis throughout this semester. My roommates Nassim Abuhalaweh, Abdulhadi Alkayyali, and Hamzah Hakkani have been instrumental in supporting me to continue working on this paper when classes got tough along with other personal and health issues arising this year. I would like to thank my mom, dad, and sister for the support they have provided me and endless meals they dropped off for me when I was too busy with my work.

Abstract

Low-grade gliomas are slow growing primary brain tumors that affect approximately 5000 adults in the US annually.[1] In 2016, the World Health Organization (WHO) restructured their classification of tumor types based on molecular and histopathological features to provide better clinical care.[2] Mutations of TP53 and 1p/19q co-deletions are characteristic features of low-grade gliomas, along with the categorization of mutated isocitrate dehydrogenase (IDH).[3] Mutations in the enzyme IDH occur in more than 80% of low-grade gliomas (LGG), astrocytoma, oligodendrogliomas and oligoastrocytomas.[4] The R132H mutant IDH is responsible for the further reduction of α-ketoglutarate to the oncometabolite D-2-hydroxyglutarate (D-2HG). There is an accumulation of D-2HG production in mIDH1 which has been shown to cause a series of epigenetic effects. Decreased expression of the immunosuppressive ligand, programmed death ligand 1 (PDL-1), by glioma cells as well as myeloid derived suppressor cells (MDSCs) are characteristics of this build up. A hallmark of the glioma microenvironment is the exhaustion of CD8+ tumor-infiltrating lymphocytes, which reduce the functionality of T cells. CD8+ T cells provide key anti-tumor immunity and are correlated with an extended survival time in brain tumors.[5] Treatment developments have been shifting toward more immunotherapeutic strategies, following the success of their use in several solid and hematologic cancers. Investigation into chimeric antigen receptors (CAR) therapies, myeloid-targeted therapies, vaccines, and immune checkpoint inhibitors are ongoing candidates. Due to the depletion of immunosuppressive genes within myeloid cells in mIDH1[6] and reduced expression of PDL-1, its inferred that mIDH1 alters multiple mechanisms of tumor infiltrating CD8+ T cell exhaustion by reducing the levels of exhaustion-associated inhibitory ligands and receptors.

Introduction

Classification of Low-Grade Gliomas (LGGs)

Low-grade gliomas are slow growing glial tumors that have the potential to evolve into other malignant forms. Patients with LGGs have shown better prognosis than those with high-grade gliomas (HGGs), however these patients remain with notable negative impacts on their quality of life. Seizures are known to be the most common side effect, along with headaches and other focal neural deficits are seen.[7] Current standard of care includes surgical intervention to resect a safe maximal amount of the tumor for molecular and genetic characterization to diagnose a proper management plan.[8] In 2021 WHO guidelines had changed to include a deeper characterization of molecular and genetic components into their grading, to place an increase in molecular diagnostics.[9] In terms of gliomas, the updated guidelines focused on the mutations in isocitrate dehydrogenase (IDH) genes.[10,11] These mutations were linked to a higher survival outcome in patients and as a result adult LGG is now by definition IDH mutant, including oligodendrogliomas and astrocytoma.[9] Further molecular profiling revealed other genetic attributes that are hallmarks of LGGs including elongation of ATRX telomere, shortening of TERT telomere, mutations within TP53, and codeletion of 1p19q.[12]

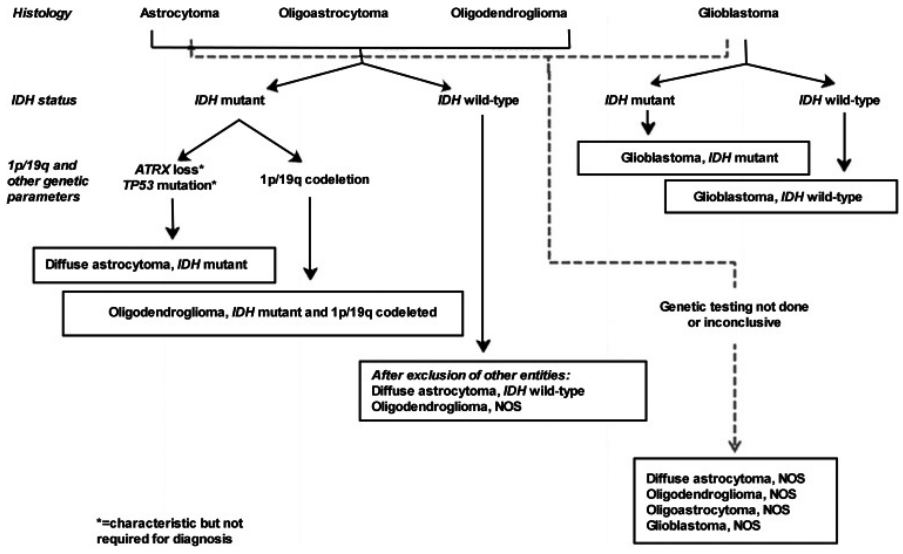

Figure 1: A simplified map for the classification of the diffuse gliomas based on histological and genetic features.[13]

Isocitrate Dehydrogenase (IDH)

Isocitrate dehydrogenase is a NADP/NAD dependent homodimer responsible for the biosynthesis of α-ketoglutarate (αKG) in the citric acid cycle. IDH1 is localized to the cytosol and peroxisome, while its counterparts IDH2 and IDH3 are localized in the mitochondria. IDH1 catalyzes the oxidative decarboxylation of isocitrate to form αKG using the cofactor nicotinamide adenine dinucleotide phosphate (NADP) to generate NADPH during the catalysis. Each of the IDH subunits consists of at least three domains, a large domain, a small domain, and a clasp domain as well as two active sites per dimer.[4] Within the active site are binding sites for NADP, isocitrate and a divalent cation, generally a calcium ion. In its inactive conformation, a regulatory loop segment blocks the binding site of isocitrate by interacting with Ser-94 of the large domain.[14] In increased concentration of isocitrate the regulatory loop segment is displaced, allowing for binding in the catalytic cleft in response to competitive binding. Thr-77, Ser-94, Asn-96, Arg-100, Arg-132, Arg-109, and Ser-278 take part in the stabilization of isocitrate within its binding site.[4]

IDH is a key regulator of the mitochondrial electron transport chain, as well as the mitochondrial NADH/NAD ratio. In order to maintain sufficient concentration of isocitrate, it is tightly regulated by the three isoforms of IDH. While within the mitochondria, isocitrate is catalyzed by IDH3. The enzyme is upregulated by increased concentration of both isocitrate and NAD or elevated levels of ATP.[15] Once the NADH concentration gets too high, IDH3 is downregulated and isocitrate concentrations will begin to increase. IDH3 may also be downregulated by increased concentration of αKG due to its production by glutamine and glutamate.[16] When IDH3 is downregulated, IDH2 will act on some of the isocitrate in the mitochondria. This will allow for the production of NADPH, granting later reduction of glutathione in defense against reactive oxidative species (ROS).[17, 18] The remaining amount of

isocitrate will be converted back to citrate and shuttled to the cytosol via citrate transport proteins. Citrate can then be converted into isocitrate in the cytosol by cytosolic aconitase and further catalyzed by IDH1 to produce αKG.[19]

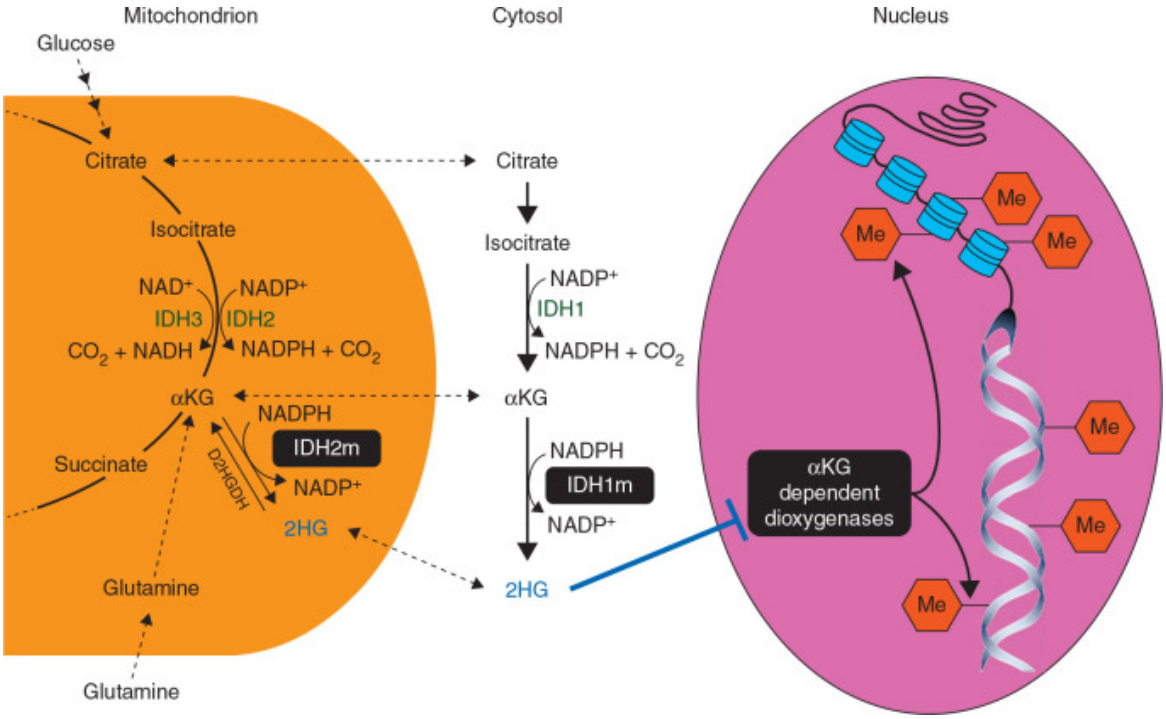

Figure 2: General mechanism of mutant IDH1/IDH2 working alongside the wild-type conformation. Production of 2HG, D-2-hydroxygluterate inhibits the activity of αKG dependent dioxygenases.[20]

With advancements in cancer genetics, it has been made known that hot spot mutations within the *IDH1* and *IDH2* genes occur in a variety of human cancers.[21] IDH3 however has not been identified as having significant mutated genes in human cancers.[22] Mutations within these genes are two distinct to arginine codons.[21] In IDH1, a missense mutation is present at Arg-132 codon causing an amino acid substitution, predominantly histidine (R132H). Other mutations have been shown where there was a substitution of cysteine, serine, glycine leucine, or isoleucine.[21,23] IDH2 also appears with a missense mutation resulting in an amino acid substitution at an arginine

homologous to that of IDH1. The mutation most commonly includes R140Q or R172K, however other mutations are present.[4, 24] The mutation in the active site of IDH1/2 results in neomorphic enzyme activity catalyzing the conversion of αKG into D2HG. Under physiological conditions, D2HG concentrations are limited by D2HG dehydrogenase (D2HGDH). D2HGDH catalyzes the reaction of D2HG to αKG. However, under the conditions of the neomorphic IDH1/2 D2HG accumulates to supraphysiolocal levels. Elevated levels of D2HG have been detected in the serum of patients with IDH-mutant gliomas.[25, 26]

Effects of 2-Hydroxygluterate (2HG)

D2HG is an oncometabolite that is formed by both IDH1 and IDH2 mutated isoforms.[27] It is structurally similar to αKG, with the only difference in the exchange of the ketone for the hydroxy group at the C2-position.[4] This degree of similarity allows D2HG to interfere with enzymes that utilize αKG, including αKG dioxygenases.[28] αKG dioxygenases are critical enzymes in degradation and genetic modification including DNA and histone demethylation, ubiquitination, hydroxylation, epigenetic alteration, and various signaling pathways.[29] At high concentrations, D2HG will out compete αKG for the active binding site within αKG dioxygenases and lead to various signaling and genetic alterations.[28]

DNA hypermethylation induced by D2HG has been shown to lead to atypical translation of oncogenes and tumor suppressor genes.[30] This plays a crucial role in the malignant transformation of IDH-mutated gliomas. The degree of DNA methylation is regulated by DNA methyltransferases (DNMT) and ten-eleven translocation (TET) proteins. There are three DNMTs, DNMT1 which is responsible in regulating DNA methylation of 5-methylcytosine (5mc) by transferring a methyl group to cytosine [31], and DNMT3a/3b which contribute to de novo

methylation.[32] TET proteins contribute to DNA methylation regulation through means of demethylation by the oxidation of 5mC to 5-hdroxymethylcytosine (5hmC), 5-formylcytosine, and 5-carboxylcytosine (5caC).[33] High concentrations of D2HG in the IDH-mutant have shown its capability to block the activity of TETs resulting in genome hypermethylation.[28,33] This is specific to cytosine-phosphate-guanine (CpG) island of the promoter region and non-promoter regions [34,35] resulting in the glioma-CpG island methylator phenotype (G-CIMP).[36,37] Patients with mutant IDH1 showed extensive hypermethylation that restated the patterns of G-CIMP positive LGGs.[38] However, this alone is insufficient in initiating glioma formation leading to believe other IDH-driven epigenetic changes make glioma cells more vulnerable to oncogenic phenotypes.[39,40] Evidence of this is shown by the 1p19q co-deletion, inactivation of tumor protein p53 (TP53), and alpha thalassemia/mental retardation syndrome X-linked (ATRX).[41,42]

Histone methylation plays a key role in transcriptional regulation and can lead to various oncogenic activity when not regulated accordingly.[43] Most histone methylation occurs on lysine and arginine residues on histone 3 and histone 4. Increased presence of D2HG mediates trimethylation of H3K4, H3K36, and H3K79 acting as transcriptional activators[44,45] while trimethylation of H3K9 and H3K27 acts as a transcriptional repressor.[46] This methylation pattern occurs due to the increased concentration of D2HG suppressing the catalytic function of JmjC-KDMs, specifically JmjC-KDM4A, JmjC-KDM4B, and JmjC-KDM4C, inducing widespread histone methylation.[47] This affects a number of biological processes contributing to cancer initiation, progression, and metastasis in various malignancies.[48] Further study into the biological processes of histone methylation patterns is still under investigation for their influence in glioma pathogenesis.

Current studies have investigated the promoter methylation of several possible immune checkpoints including PDL-1, PDL-2, and PD-1 in LGGs. The role of PD-1 is responsible in promoting self-tolerance by suppressing T-cell activity. When bound to PDL-1 or PDL-2, PD-1 initiates apoptosis in antigen specific T-cells and reducing programmed cell death in regulatory T-cells (Tregs).[49] DNA promoter methylation has shown a number of significant factors for overall survival in patients with LGGs, resulting in functional tumor-specific T-cells initiating increased antitumor immune response.[50]

Blood-Brain Barrier

The blood-brain barrier (BBB) is a complex structure in regulating the exchange of biological components between the blood and the brain interfaces sustaining homeostasis.[51,52] This barrier is secured by endothelial cells adhered by tight junctions and pericytes embedded in the basement membrane.[53,54] Although the BBB is shown to allow the transport of essential nutrients and maintain a stable brain environment, it is highly selective under normal physiological conditions.[55,56] Molecules over 400 Da that form more than eight hydrogen bonds are not able to pass the BBB. Other molecules that do fit the criteria may pass in small fractions dependent on their lipid solubility.[51,56] However, in the presence of a tumor the BBB is compromised due to associated inflammation. The inflammation causes changes in cellular components in the anatomy and function of the barrier, altering the permeability of blood vessels in the brain. [53,57] This inflammation is driven by the activation of hypoxia, abnormal angiogenesis, and tissue remodeling, all of which being characteristics of gliomas.[54,55,58]

During gliomagenesis, numerous pathways are activated triggering inflammatory responses in the brain microenvironment. The glioma microenvironment is known to be

extensively hypoxic and necrotizing, causing mediation by hypoxia-inducible factor-alpha (HIF-α).[54,55,58] This regulator is a driving factor in tumor growth and disruption of the BBB. HIF-α regulates the expression of angiogenic and inflammatory factors including vascular endothelial growth factor (VEGF).[60,61] VEGF is responsible for the activation of angiogenesis which entails the disruption of cellular barrier pulling endothelial cells to form new capillaries and fewer tight junctions.[61,62] This results in the increased infiltration of cellular and plasma components into the brain environment, eliciting further inflammation and disruption of the BBB.[63]

In a compromised BBB the natural immune surveillance by effector immune cells begins to excessively infiltrate and amplify the inflammatory responses.[64] Inflamed immune cells such as tumor-associated macrophages produce tumor necrosis factor-alpha (TNF-α).[58,65.66] TNF-α is an inflammatory cytokine that will promote the expression of inflammatory molecule within cells, leading to necrosis or apoptosis.[65,66] Other cells releasing cytokines will increase the inflammatory immune environment disrupting the BBB including astrocytes, microglia, and endothelial cells secreting transforming growth factor (TGF-β) and metalloproteinases (MMPs).[65,67] Increased TGF-β signaling reduces the expression of cell adhesion in pericytes and endothelial cells, weakening the attachment of the BBB.[64,68] MMPs will alter the function of the basement membrane where pericytes are embedded due to cleavage of the basal lamina by activated microglia.[66,68]

Tumor Immune Microenvironment

The central nervous system (CNS) is known to be classified as “immune privileged”, however during gliomagenesis the neuroinflammation that compromises the BBB causes for the infiltration of immune cells.[70, 52] A variety of immune cells within the glioma tissue begins to

influence interactions between the tumor and the host, allowing the microenvironment to be more susceptible to suppression and evasion of immune responses at varying levels.[71] This also occurs in peripheral antitumor immune cells, where they are often reprogrammed into specific immunosuppressive phenotypes in the tumor immune microenvironment.[72] Infiltrates include a number of immune cells such as myeloid cells, T cells, B cells, and dendritic cells.

Microglia and tumor associated macrophages (TAMs) are both categorized as myeloid cells, however the localization of the two cells are independent of one another. Microglia takes resident within the brain with self-renewal ability along with prolonged cellular longevity and proliferation.[73] TAMs are derived from hematopoietic stem cells from within the bone marrow that can migrate and infiltrate the BBB into the glioma microenvironment.[74] Under normal physiological conditions microglia and peripheral macrophages (derived as monocytes) activate proliferation and maintain regulation of the CNS immunological homeostasis.[75] Under the physiological stress of glioma microenvironment, TAMs begin to adopt an M2 phenotype activating immunosuppressive pathways promoting tumor growth and progression.[76,77] Recruitment of these cells is in response to increase production of chemoattractant – CCL2, CX3CL1, colony-stimulating factor-1 (CSF-1) and stromal cell-derived factor 1 (SDF-1) – within the glioma microenvironment.[76,77,78] As a result, once with in the glioma microenvironment further cellular signaling occurs eliciting the release of a multitude of cytokines form the TAMs including TGF-β, stress inducible factor-1 (STI-1), IL-6, IL-1β, IL-10 and epidermal growth factor (EGF), promoting positive feedback in proliferating glioma cells and inhibiting T cell activity.[75,76]

Myeloid-derived suppressor cells (MDSCs) are a heterogeneous population of immature myeloid cells derived from monocytic (M-MDSCs) or granulocytic (PMN-MDSCs) origin.[11] MDSCs of both origin express high levels of immune suppressive molecules and inhibit antitumor

immunity. Although it's shown that M-MDSCs have a greater potency in immunosuppressive capability, PMN-MDSCs make up a greater portion of the MDSCs within the glioma microenvironment.[80] Glioma cells utilize various cytokines in order to drive infiltration and expansion of MDSCs such as CCL2, CXCL8, SDF-1, CXCL2, and IL-6, PGE-2, IL-10, VEGF, GM-CSF, respectively.[80,81] In the glioma microenvironment MDSCs have the capability of being potent inhibitors of CD4+ and CD8+ T cells and other significant immunosuppression.[82,83] This is triggered by multiple mechanisms working in conjunction including induction of oxidative stress, inhibition of T cell migration, expression of T cell inhibitory ligands, and depletion of necessary T cell metabolites.[79,80]

Of all the other immune infiltrates, the largest lymphocyte population is T cells, which are key regulators of anti-tumor immunity.[84,85] T cell priming occurs outside the glioma microenvironment in the cervical draining lymph nodes.[63] Here an antigen is loaded on dendritic cells (DC) and presented to CD8+ T cells via MHC class I molecules, transforming them into cytotoxic anti-glioma CD8+ T cells (CTLs).[86,87,88] Several studies have shown however that the vast majority of CD8+ T cells that are in the TME are characterized as exhausted, exhibiting a hypo-responsive activity.[88] Exhaustion occurs from chronic antigenic exposure under sub-optimal conditions. Exhausted T cells are characterized by the upregulation of various co-inhibitory receptors including PD-1, CTLA-4, LAG-3, and TIM-3 on the T cells.[85,90,91] T cells in this state will secrete lower concentrations of effector cytokines and therefore provide reduced antitumor immunity.[89] CD4+ T cells however are proposed to mediate anti-tumor immunity through assisting CD8+ CTLs. These cells mediate CD8+ CTLs by secreting effector cytokines such as interferon-γ (IFN-γ) and tumor necrosis factor-α (TNF-α).[79] CD4+ T cells are highly versatile and may differentiate into a number of subtypes, the most studied being regulatory T cells (Tregs).[92] Tregs

establish immunosuppressive activity and promote anti-tumor growth in the glioma microenvironment.[79] Therefore, providing a possible target site to further glioma immunotherapy.

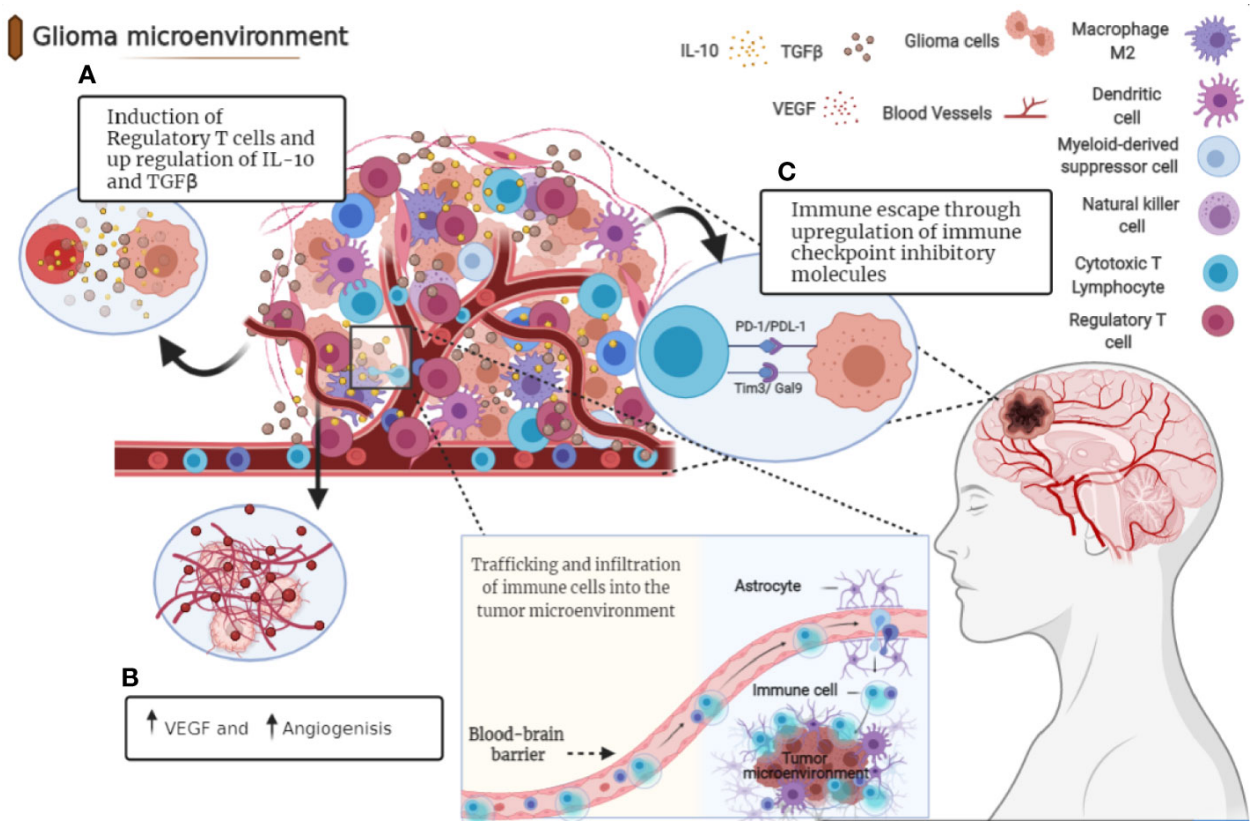

Figure 3: Tumor cells release a number of signaling molecules that elicit immunosuppression by various cellular components in the glioma microenvironment. **(A)** Regulatory T cells suppress T cell activity promoting apoptosis through section of cytokines such as IL-10 and TGFβ. **(B)** Angiogenesis is a hallmark of glioma development mediated by vascular endothelial growth factor (VEGF). **(C)** Immune checkpoints suppress T cell functionality in the microenvironment through specifics mechanisms.[93]

T-Cell Exhaustion and Immune Checkpoint Inhibitors

Naturally, when a naïve CD8+ T cell is encountered by an antigen presented by a dendritic cell, they differentiate into CD8+ CTLs in order to attack and manage the antigen and its source. Once completed, most of these cells become apoptotic while a few remain as T memory cells (Tmems).[94,95] However, during tumorigenesis T cells differentiation is found to be interfered with

and promote a hyporesponsive state known as exhaustion.[96] Exhaustion relates to activated T cells that are now downregulated in effector activity. Exhausted CD8+ T cells play a pivotal role in the glioma microenvironment where antigen exposure is consistent and chronic inflammation is present.[94] In addition to their loss of activity, the expression of multiple inhibitory receptors is a key determinant of T cell exhaustion, such as PD-1, CTLA-4, LAG-3, and TIM-3. [97]

Understanding the downstream mechanisms of these inhibitory receptors would allow us to investigate how they regulate specific cellular functions. Research into these receptors has begun to show promising results in terms of relation to T cell exhaustion. Examples include PD-1 and LAG-3, where they affect survival/proliferation of exhausted CD8+ T cells[98,99,100,101] and cell cycle progression[102,103], respectively. However, it has been shown that these receptors may impair T cell response in different ways.[94] PD-1 ligation for example demonstrates mechanisms of both suppressing and inducing signaling as well as gene expression involved in inhibition of T cell function.[104,105] CTLA-4 is also shown to exhibit dual effects such as outcompeting CD28 for costimulatory ligands as well as diminishing signaling and gene expression.[104] Future studies are still required to understand and map intracellular mechanisms related to these surface inhibitory receptors and their ligands.

Evading immune surveillance within the glioma microenvironment has proven to be a challenge with the development of a host of mechanisms that induce a state of immune tolerance.[106] One of these mechanisms involves the use of the characteristically upregulated inhibitor receptors known as immune checkpoints.[107] Clinical trials have implicated treatments directed towards these T cell inhibitory receptors using immune checkpoint inhibitors.[108,109] Creating these immune checkpoint blockades, hope to allow for a decrease in tumor progression and reinvigorate moderately exhausted CD8+ T cells while allowing others to reach a terminal state.[96] The genetic

variability that forms this exhaustive environment is unique to each tumor and has specific dynamic interactions with immune checkpoints.[110] Some immune checkpoint inhibitors have proven to be ineffective on their own, however a combination improved this result.[96] New WHO guidelines of establishing tumor type and grading through means of genetic and molecular characterization assisted this need and provides sufficient diagnostic care in designing a rational combination therapy to specific tumor types.

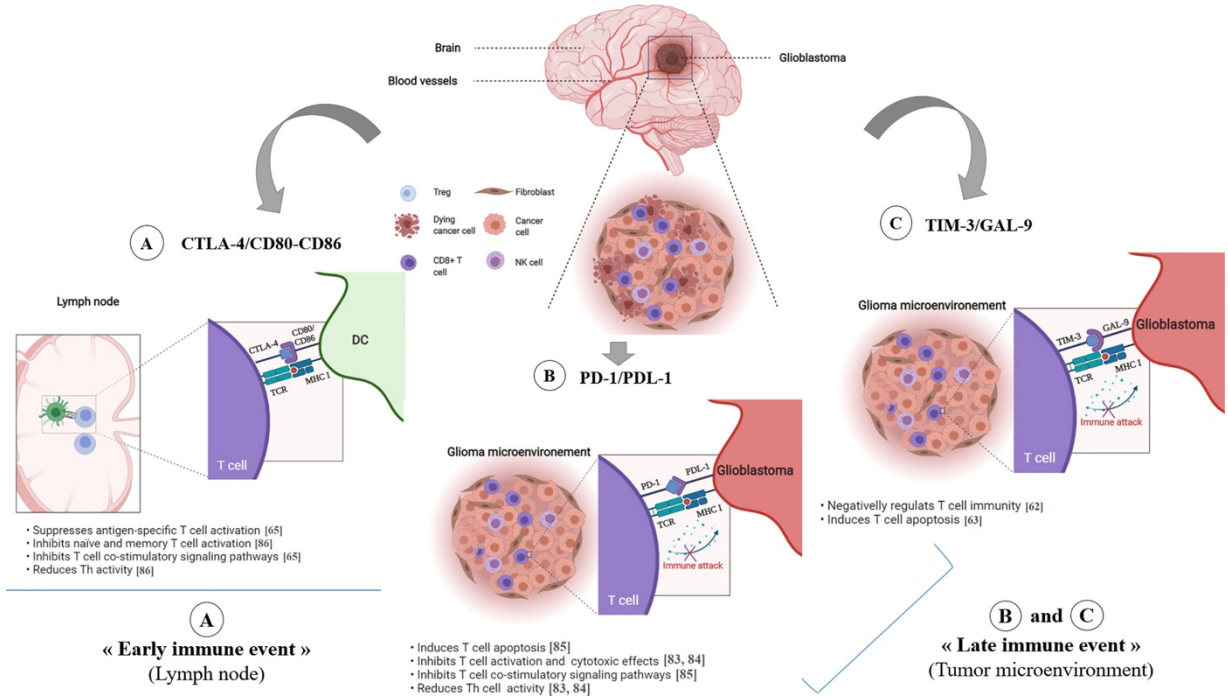

Figure 4: Immune checkpoint inhibitors and co-receptors/ligand activity in glioma development.[93]

Materials and Method

Sleeping Beauty Mouse Glioma Models

The mIDH glioma mouse models that are genetically engineered in this experiment were created using the Sleep Beauty Transposon System. Using this method of genetic engineering allows for the incorporation of genetic lesions into the genome of neonatal mice. The tumor is then

allowed to develop *de novo* intracranially from neuronal progenitor cells. Plasmids encoding these genetic lesions include sleeping beauty transposase and luciferase, a short hairpin against p53 (shp53), an NRAS-G12V activating mutation (NRAS), a short hairpin against ATRX (shATRX), and mutant IDH-R132H. Two genotype combinations of these mouse glioma models were developed, wt-IDH1 (shp53, NRAS, and shATRX) and mIDH1 (shp53, NRAS, and shATRX, IDH1-R132H). The transfection mixture was incubated for 20 minutes upon preparation and then maintained on ice until use. The lateral ventricle (1.5 mm AP, 0.7 mm lateral, and 1.5 mm deep from the lambda) of the neonatal mice was injected with 0.75 microliters of one of the two genotype (wt-IDH1 and mIDH1) plasmids. at a rate of approximately 0.5 microliter per minute.

Neurosphere Culturing

Primary mouse glioma neurospheres are generated using the brain tumors of sleeping beauty mouse models. The mice are euthanized by transcranial perfusion with Tyrode's solution only and harvested for the brain. Once excised, the brain is examined under an epifluorescence microscope. The tumor that is generated by the Sleeping Beauty Transposon System expresses GFP and Katushka which will allow for visualization of the tumor versus healthy tissue. The tumor is dissociated using a non-enzymatic cell dissociation buffer and filtered through 70 micrometer strainers. The filtrate is maintained in neural stem cell medium in T-75 flask, B-27 supplement, N-2 supplement, penicillin-streptomycin (100 U/ml) at 37-degree Celsius, 5% CO_2. Fibroblast and epidermal growth factor (FGF and EGF) are added twice weekly at 1 microliter of 20 nanogram per microliter stock per milliliter of medium. After 3 days in culture a mixed population of three varying morphologies may be identified in the flask: adherent cells, dead cells, and glioma neurospheres. The neurosphere population can be identified as clusters that are floating and will be isolated into a new T-75/T-25 flask.

Implantation

Glioma neurospheres are collected from the T-75 flasks for 5 x10^4 cells of wtIDH1 or mIDH1 to be transfected into the right striatum of each mouse. Mice are anesthetized using a combination of ketamine and dexmedetomidine totaling 100 microliters. The surface of the skull is shaved and cleaned with iodine once placed on the stereotactic for implantation. The coordinates for implantation are 0.5 mm anterior and 2.0 mm lateral from the bregma and 3.0 mm ventral from the dura. Neurospheres are then injected at a rate of 1 microliter per minute. Once completed and sutured, the mice were given a combination of buprenorphine (0.1 mg/kg) and carprofen (5 mg/kg) for analgesia.

In-vivo Imaging

In-vivo bioluminescence was measured post implantation using an IVIS spectrum imaging system. The following settings were set when using the IVIS spectrum: automatic exposure, large binning, and aperture f=1. The mice were anesthetized using a combination of oxygen and isoflurane (1.5-2.5% isoflurane). To monitor the tumor formation and progression in the adult mice, 100 microliters of luciferin solution was intraperitoneally injected. To quantify the luminescence, Living Image Software was used. A region of interest (ROI) was defined as a circle of the heads of the mice, and luminescent intensity was measured in units of $sr{\times}photons/cm2$. Two images were collected, the first after 3 minutes of injection and the second after 5 minutes injection, with the maximal intensity being recorded. Regarding survival studies, animals were monitored for symptomatic characteristics such as ataxia, impaired mobility, hunched posture, seizures, and scruffy fur. Animals displaying these symptoms and/or displayed a luminescent intensity greater than 10^8.

Single Cell Suspension and Purification

Several types of tissue were collected: brain, lymph nodes, spleen, blood. To isolate the tumor-infiltrating immune cells, the mice were euthanized, and the brain was extracted. The tumor mass within the brain was dissected and placed in DMEM media containing 10% FBS. The tumor was strained through a 70-micrometer strainer attached to a 50-milliliter conical tube using a pistol and 30-40 milliliters of DMEM media containing 10 % FBS to ensure minimal cell loss. The cells were then centrifuged, and the supernatant was discarded. The pellet was resuspended in 7 milliliters of media in a 15-milliliter conical tube and 3 milliliters of 90% isotonic percoll. In order to create the density gradient 1 milliliter of 70% percoll was added to the bottom of the 15-milliliter tube carefully using a serological pipette. The combined solution with the distinct layers were centrifuged an 800 x g for 20 min at room temperature, and the tumor-infiltrating immune cells were collected cautiously from the white band found in-between the two layers. To isolate spleenocytes, freshly extracted spleens are isolated and are passed through a 70-micrometer strainer using a pistol. The strainer was washed with 30-40 milliliters of DMEM media to ensure minimal cell loss. To collect the blood from the mice before coagulation, the sample was collected directly after/during euthanasia. The mice are placed under anesthesia and the chest cavity is open where the heart is visible. An intracardiac stick was performed to euthanize the mice and collect the blood sample with a pipette transferred into an EDTA-coated tube. With the chest cavity still open the superficial and deep cervical lymph nodes were collected and passed through a 70-micrometer strainer using a pistol. The strainer was washed with 30-40 milliliters DMEM media. The blood, lymph nodes, and spleenocytes were centrifuged, their red blood cells were lysed using RBC lysis buffer (1 milliliter for spleenocytes and lymph nodes, 8 milliliters for blood). The

samples were neutralized with DPBS for a total volume of 10 milliliters. The cells were centrifuged and ready for antibody preparation.

Flow Cytometry

In preparation of flow cytometry, the cells are prepped for staining. All the staining was performed at 4-degree Celsius and minimal exposure to light to minimize cellular metabolic activity and marker expression changes during the process. The cells are resuspended in a PBS and viability dye, Amcyan, to label for dead cells and incubated for 20 minutes, then centrifuged at 1500 rpm for 5 minutes. After being washed and centrifuged with PBS, the cells are stained with FC Block (CD16/CD32) to block non-specific binding, then centrifuged at 1500 rpm for 5 minutes and washed with PBS. Cells were then stained with fluorescent conjugated antibody cocktails and incubated for 30 minutes. The antibody cocktail included CD45, CD8, CD3/TCRβ, CD4, CD8, PD-1, CTLA-4, TIM-3, and LAG-3. After which, they were washed with 2X flow sheath fluid. Samples were then ready for data collection on FACSAria II flow cytometer and analyzed fusing FlowJo version 10.

Mass Cytometry

All antibodies for mass cytometry were titrated to ensure optimal concentrations for each antibody to recognize ideal separation between positive and negative population. Single cell suspensions were obtained as described previously. Cells were then stained with 1.67 micromolar of Cisplatin for 5 min at room temperature to identify and label dead cells. Afterwards, the cells were quenched with 5x volume of MaxPar Cell Staining Buffer, cells were counted and centrifuged at 300 x g for 5 minutes. Approximately 2-3 million cells were stained with a cocktail of metal-conjugated surface antibodies, which were added in appropriate concentrations according to the titration performed and incubated for 30 minutes. Samples underwent a washing process with

MaxPar Cell Staining Buffer, and then were fixed and permeabilized in 1.6% of freshly prepared paraformaldehyde. The samples were incubated for 10 min at room temperature and washed. Cells were then stained with an intracellular antibody cocktail and incubated for 30 minutes, then washed using MaxPar Cell Staining Buffer and resuspended in 2 milliliters of intercalation solution for 24 hours at 4-degree Celsius (in order to label the nucleated cells). Before loading the samples, cells were washed once more with MaxPar water, counted, and diluted to the appropriate concentration. Cytobank software was used to perform population gating and advanced data analysis.

Single cell-RNA sequencing

Tumors were harvested from either wtIDH1 or mIDH1 SB mice and kept in RPMI media. The tumor was cut up into smaller pieces and transferred into a 50-milliliter tube to be centrifuged at 1500 RPMI for 5 minutes. The pellet was resuspended in 1 milliliter of Accutase to dissociate the tissue. After 5-10 minutes at 37 degrees Celsius, the Accutase was neutralized with 9 milliliter RPMI media. Further debris and dead cells were removed using the dead cell removal column and was twice with PBS. The remaining cells were counted and resuspended at a concentration of 1000 cells per microliter. Cell viability was determined by an automated cell counter to be greater than 90%.

For human samples, the freshly isolated primary tumor tissue is kept in DMEM/F12 media and cut into small pieces until a homogenous solution is obtained. As done previously, cells are dissociated using Accutase in two-cycles of 5 minutes each until single-cell suspension is obtained. Initial purification was done by passing the cell suspension through a 70-micrometer strainer to remove any debris and connection tissue, followed by being lysed with RBC lysis buffer. The remaining suspension was passed through a dead cell removal column to ensure purity of at least 90% live cells to be considered adequate for single cell RNA-sequencing.

Results

Identifying Exhaustion Markers

Expression of exhaustion markers were first visualized prior to beginning treatment. The purpose of this is to ensure the presence of these markers on CD8+ T-cells. Other studies have shown data where presence of PD-1, CTLA-4, LAG-3, and TIM-3 were notable on T-cells. Each of these markers have considerable effects on the immune system, specifically T cell activity. Two groups of mice were prepared for this experimental design (shown in Figure 3), each consisting of 5 mice. Neurospheres were prepared in accordance with the group, group 1 received NPA (wtIDH1) neurospheres and group 2 received NPAI (mIDH1) neurospheres. Post implantation, the mice were monitored until they were late stage symptomatic. Once the mice were euthanized, they were harvested from the brain, lymph nodes, spleen, and blood and processed for flow cytometry with the exhaustion staining panel: Amycan, CD45, CD3/TCRβ, CD4, CD8, PD-1, CTLA-4, LAG-3, and TIM-3.

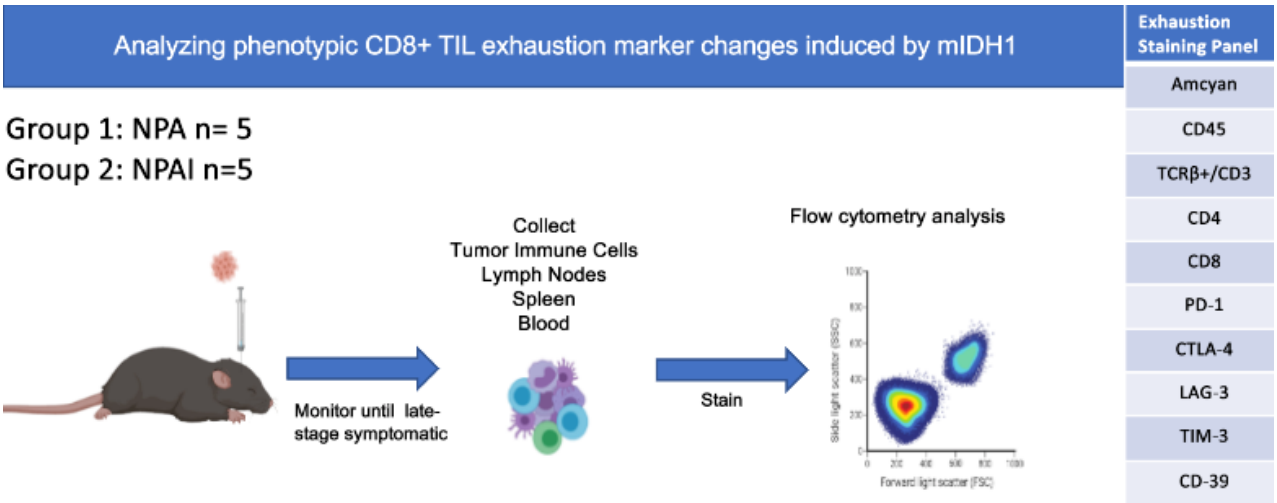

Figure 5: Experimental design in identifying CD8+ TIL exhaustion markers induced by mIDH1. Mice were implanted with NPA or NPAI neurospheres, then harvested for the tumor, lymph nodes, spleen, and blood, and analyzed against the listed exhaustion staining panel by flow cytometry.

Tumor Microenvironment

Analysis of the flow cytometry data shows a significant difference in live immune cell infiltration in the NPAI models as compared to the NPA. This is shown by the decreased frequency of live CD45+ cells in NPA (73.3%) relative to NPAI (44.7%) (Shown in Figure 5.A and 5.B). Although sample size was not optimal, indication of T cells was present in the NPA and NPAI model. The NPA exhibited a 10.8% frequency of the live immune cells to be T cells while the NPAI model identified only 7.56%. This is expected; however, the frequency of the T cell population was much lower than expected. Distinct populations of both CD4+ and CD8+ T cells were identified from the T cells using CD4 and CD8 antibodies. The NPA model displayed a 46.2% frequency and 38.1% frequency in CD4+ and CD8+ T cells, respectively, while the NPAI model displayed a 41.4% and 32.8% frequency. Due to the low frequency of total live T cells, there was a limited population of CD8+ T cells to collect accurate exhaustion marker data. High expression of PD-1 receptors was found on CD8+ T cells, with similar frequency found in both populations. Both of the NPA and NPAI model had over 90% of their T cell population express PD-1. CTLA-4 markers showed virtually no expression of CTLA-4 receptors on CD8+ T cells with less than 1% present in either the NPA or NPAI model. Expression of TIM-3 showed significant differences between the two groups, however once again overall expression within the CD8+ population was low. Expression of TIM-3 was nearly twice as much in the NPAI model with a relative frequency of 7.03% compared to the NPA with only a 3.76% frequency. Expression of LAG-3 receptors was once again higher in the NPAI than the NPA identifying 40.1% and 58.1% frequency of CD8+ T cells, respectively.

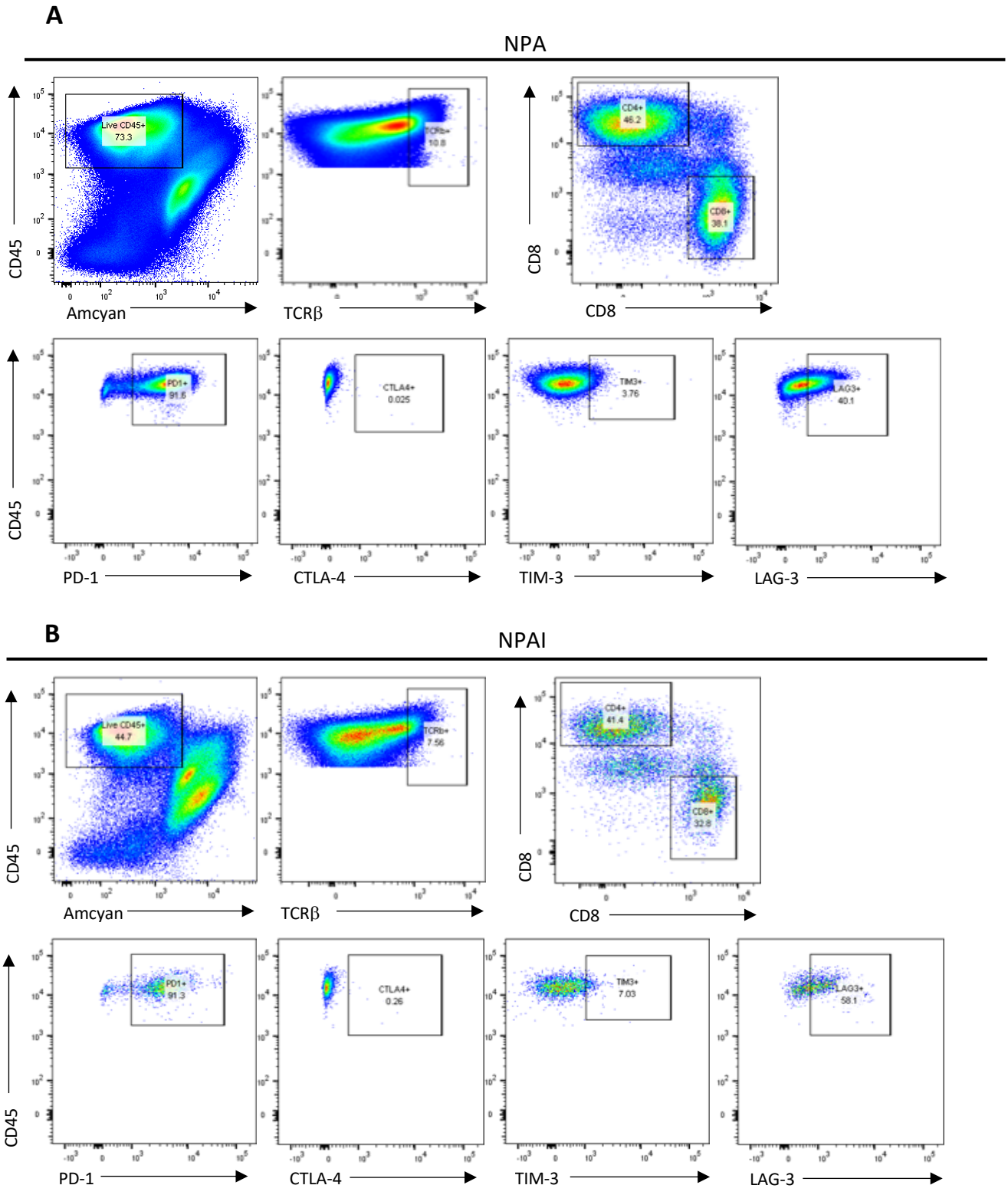
A
NPA
Live CD45+
73.3
CD45
Amcyan
TCRβ
CD4+
46.2
CD8+
38.1
CD8
CD8
PD1+
91.6
CTLA4+
0.025
TIM3+
3.76
LAG3+
40.1
CD45
PD-1
CTLA-4
TIM-3
LAG-3
B
NPAI
Live CD45+
44.7
CD45
Amcyan
TCRβ
CD4+
41.4
CD8+
32.8
CD8
CD8
PD1+
91.3
CTLA4+
0.26
TIM3+
7.03
LAG3+
58.1
CD45
PD-1
CTLA-4
TIM-3
LAG-3

C

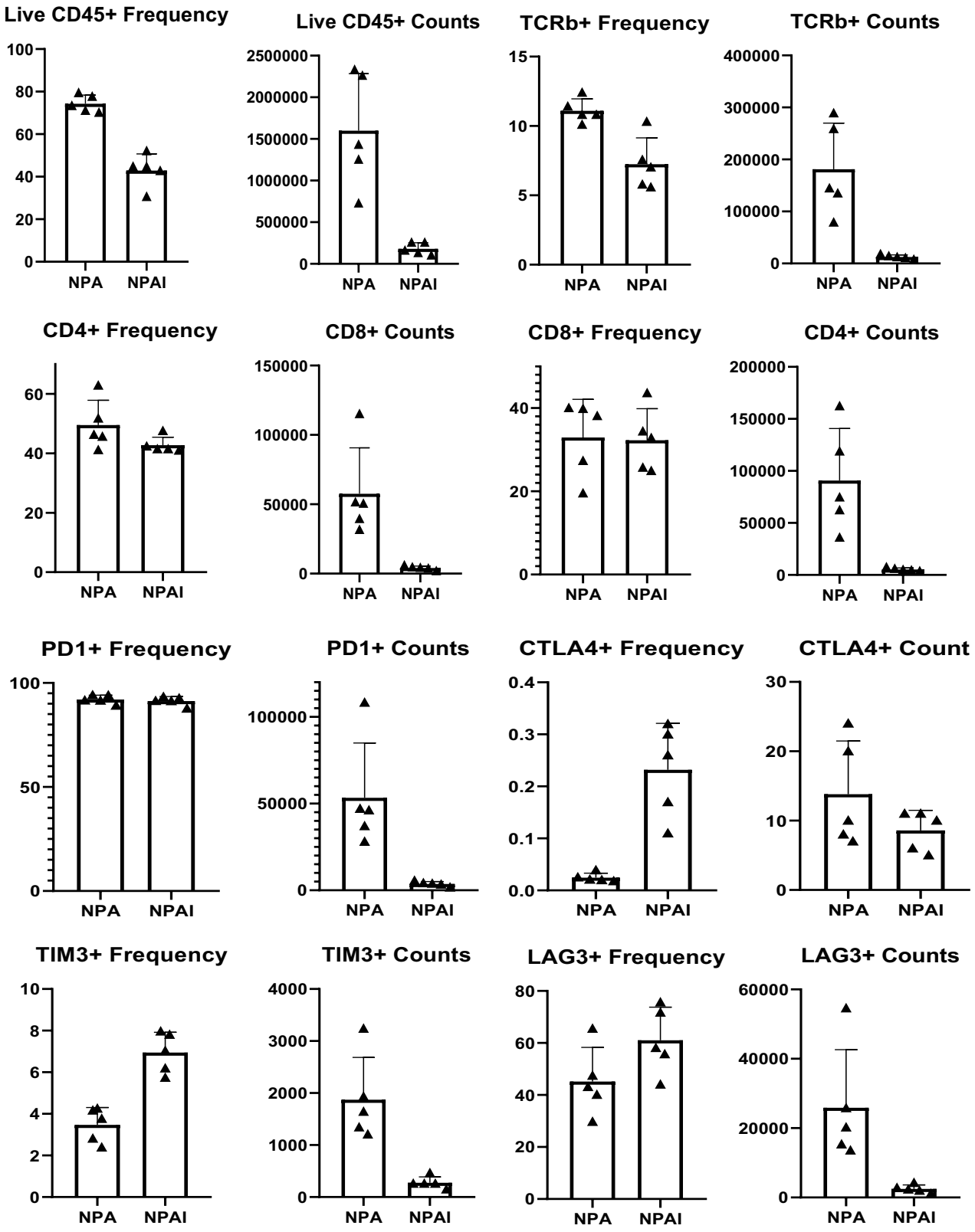

Figure 6: Data collected of tumor microenvironment for CD8+ TIL exhaustion markers induced by mtIDH1. **(A)** and **(B)** represent the flow cytometry data of the NPAI and NPA model. **(C)** illustrates a graphical representation of the data.

Lymph Nodes

Analysis showed that difference in live CD45+ cells present in the lymph nodes of both models to not be statistically different. The graphs, shown in Figure 7.C, provide the evidence of no statistical difference in the frequency or number of cells being present in the FlowJo Software. However, when focusing on the T cell population with TCRβ antibodies, there was statistical difference shown in the frequency of the two models. NPA showed 55.7% of the live immune cell population to be T cells while the NPAI model only showed 36.6% to be T cells (shown in Figure 7.A and 7.B). Although the frequency of the population was statistically different, the number of cells being present was not (shown in Figure 7.C). Focusing deeper into subpopulation of T cells, using CD4 and CD8 antibodies, we see no statistical difference between the NPA and NPAI model in frequency or in the number of cells present (shown in Figure 7.C). The identified frequency for the CD4+ and CD8 populations for the NPA model were 44.6% and 50.5%, respectively, and for the NPAI model were 50.1% and 41.9% (shown in Figure 7.A and 7.B). From here we focused on the CD8+ population for exhaustion markers. When identifying PD-1 receptors, three populations were collected, total PD-1+ cells, PD-1 intermediate cells, and PD-1 high cells. Whether the cells were high or intermediate was dependent on their expression levels as distinct cluster populations were visible for both (shown in Figure 7.A and 7.B). The frequency of the three populations in the NPA model were 53.7%, 45.8%, and 4.96%, respectively, while the NPAI model frequencies were 27.8%, 15.1%, and 10.8%, respectively. There was no statistical difference in the frequency of PD-1 high cells, however, there was statistical difference in the PD-1 total population and PD-1 intermediate (shown in Figure 7.C). Expression levels of CTLA-4, TIM-3, and LAG-3 receptors showed very low frequency, all of them displaying less than 1%. CTLA-4+ frequencies in the NPA and NPAI models were 0.33 and 0.088 with statistical difference in the frequency and cell count.

TIM-3 frequencies in the NPA and NPAI models were 0.16 and 0.19 with no statistical difference between in either frequency or cell count. And lastly, LAG-3 frequencies in the two models were 0.68 and 0.25 with no statistical difference in frequency or cell count.

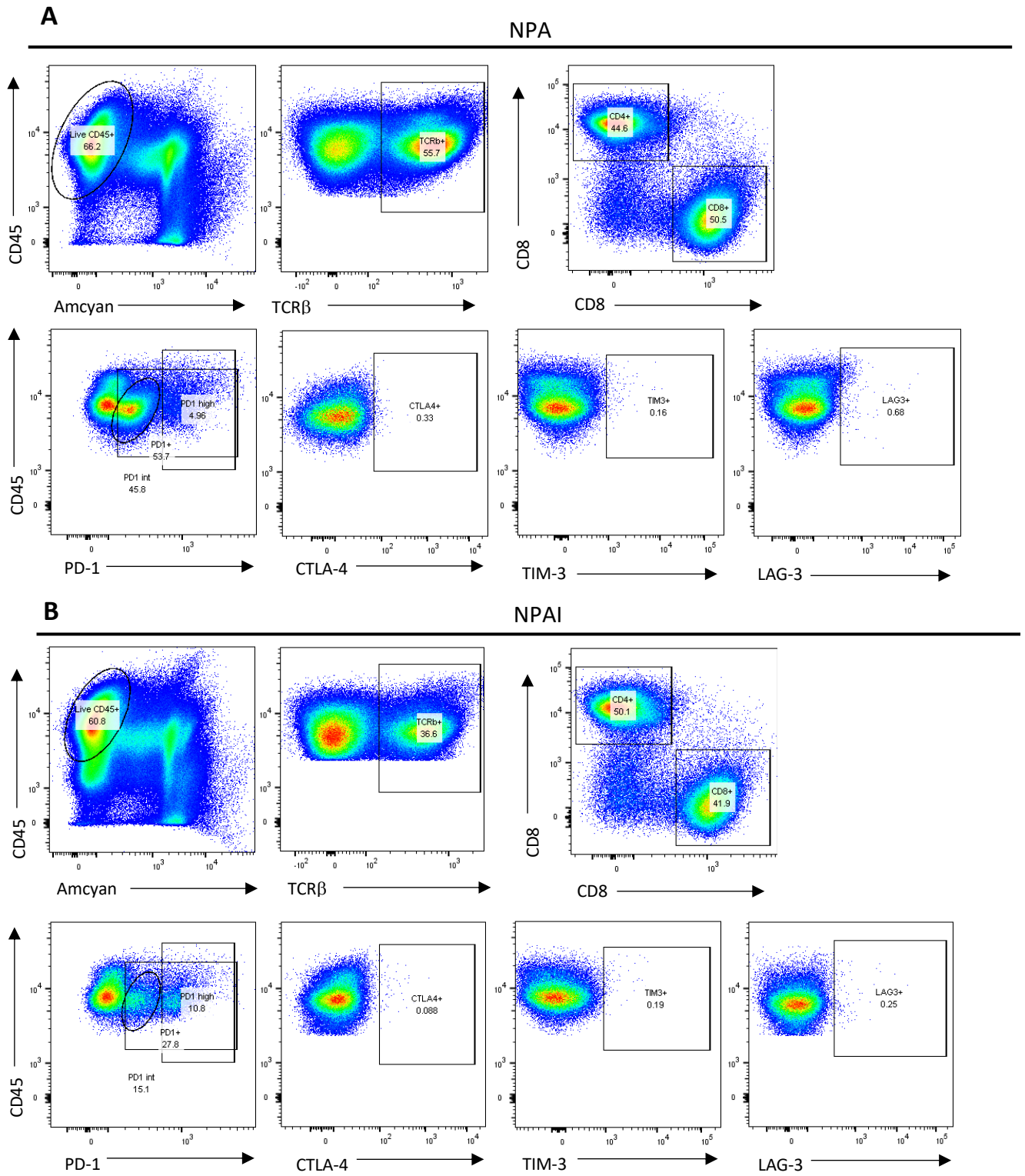
A
NPA
Live CD45+
66.2
CD45
Amcyan
TCRb+
55.7
TCRβ
CD4+
44.6
CD8+
50.5
CD8
CD8
PD1 high
4.96
PD1+
53.7
PD1 int
45.8
PD-1
CTLA4+
0.33
CTLA-4
TIM3+
0.16
TIM-3
LAG3+
0.68
LAG-3
B
NPAI
Live CD45+
60.8
TCRb+
36.6
CD4+
50.1
CD8+
41.9
PD1 high
10.8
PD1+
27.8
PD1 int
15.1
CTLA4+
0.088
TIM3+
0.19
LAG3+
0.25
C
Live CD45+ Frequency
Live CD45+ Counts
TCRb+ Frequency
TCRb+ Counts
NPA
NPAI

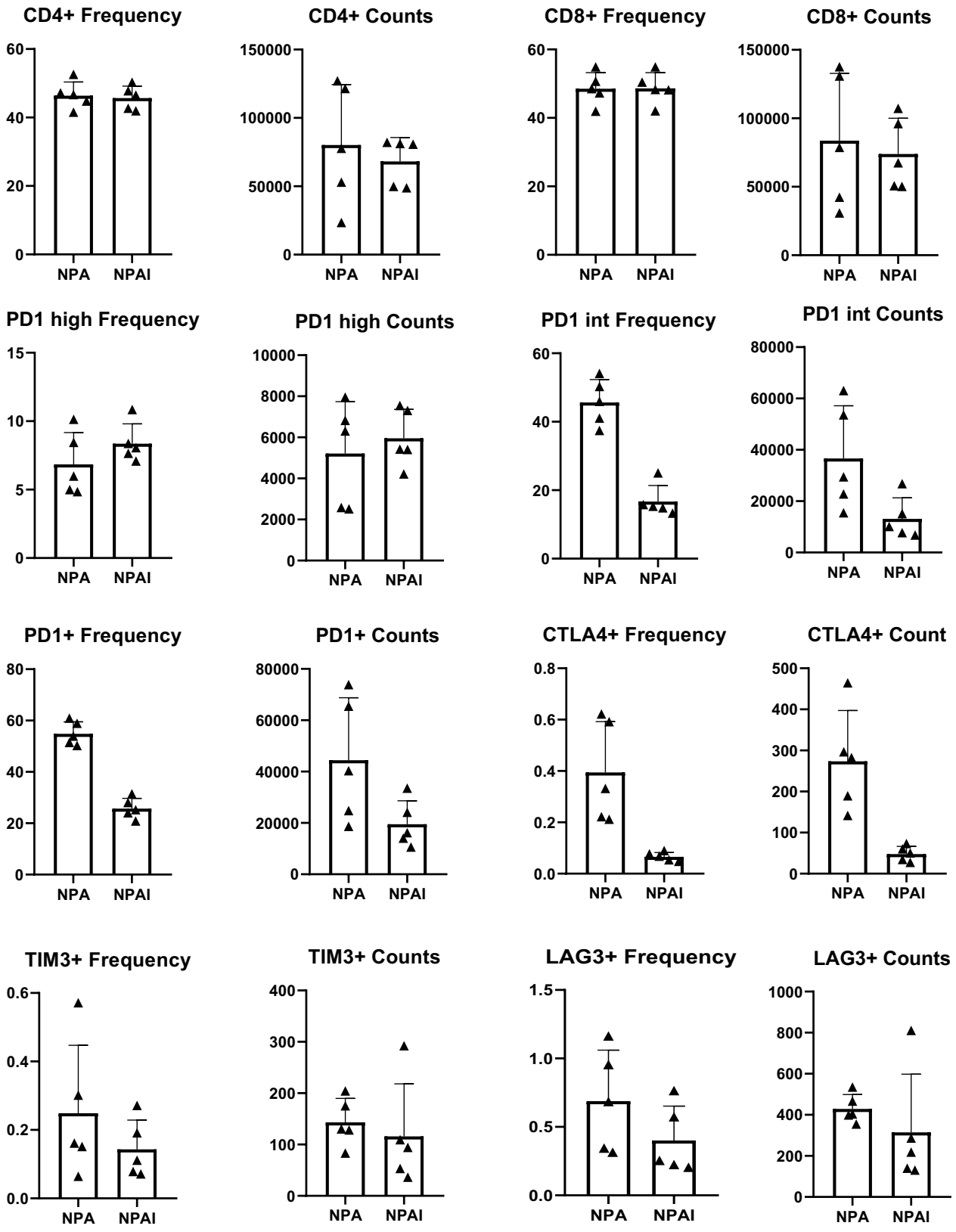

Figure 7: Data collected of tumor microenvironment for CD8+ TIL exhaustion markers induced by mtIDH1. **(A)** and **(B)** represent the flow cytometry data of the NPAI and NPA model. **(C)** illustrates a graphical representation of the data.

Spleen

Analysis of spleenocytes with CD45 antibodies indicated a significant statistical difference between the NPA and NPAI models. The NPA model consisted of only 7.29% live CD45+ cells while the NPAI model 31.5% live CD45+ cells (shown in Figure 8.A and 8.B). From these populations we identified the percentage of T cells present within these live immune cells. There was a statistical difference in the concentration of T cells that were present as well, with a higher frequency in the NPA model when the CD3 antibody was used. The NPA model indicated a 66.1% frequency within the live CD45+ population, while the NPAI only indicated a 35.0% frequency (shown in Figure 8.A and 8.B). At this we divide into looking at subpopulations of T cells, specifically those that are CD4+ or CD8+, with CD4 and CD8 antibodies. The CD4+ population of T cells showed a 66.2% frequency in the NPAI and a 42.2% frequency in the NPA (shown in Figure 8.A and 8.B). More importantly for this study, the CD8+ population showed a greater frequency present in the NPA model with 43.8% while the NPAI was only 23.7% (shown in Figure 8.A and 8.B). Now we can focus on the possible exhaustion marker population of the live CD8+ T cells. Three distinct populations were measured in respect to identifying PD-1 receptor expression, PD-1 total, PD-1 intermediate, and PD-1 high. The NPA model presented with a 36.6% of total PD-1 expression, 22.6% of intermediate PD-1 expression, and 13.5% of high PD-1 expression (shown in Figure 8.A and 8.B). CTLA-4 expression showed a notable difference between the two models. The NPA model exhibited 8.1% of the live CD8+ T cells to express CTLA-4, while the NPAI only exhibited 1.45% (shown in Figure 8.A and 8.B). Exhaustion markers LAG-3 and TIM-3 showed low expression in both the NPA and NPAI. In terms of TIM-3, the NPA model showed 1.74% of expression and the NPAI showed 0.69% (shown in Figure 8.A and 8.B). LAG-3 showed 2.86% expression frequency while NPAI showed only a 0.55% frequency (shown in figure 8.A and 8.B).

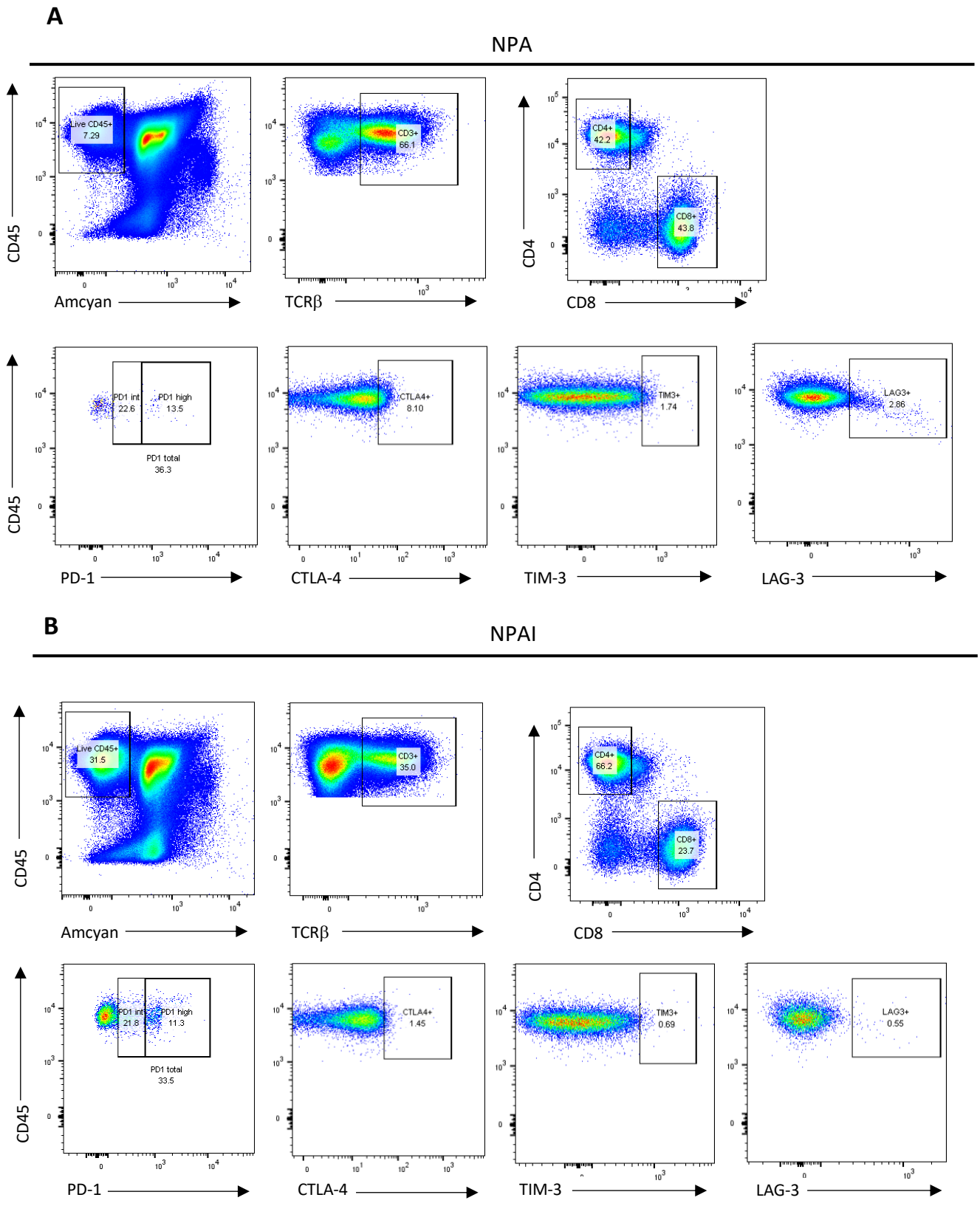
A
NPA
Live CD45+
7.29
CD3+
66.1
CD4+
42.2
CD8+
43.8
CD45
Amcyan
TCRβ
CD4
CD8
PD1 int
22.6
PD1 high
13.5
PD1 total
36.3
CTLA4+
8.10
TIM3+
1.74
LAG3+
2.86
PD-1
CTLA-4
TIM-3
LAG-3
B
NPAI
Live CD45+
31.5
CD3+
35.0
CD4+
66.2
CD8+
23.7
PD1 int
21.8
PD1 high
11.3
PD1 total
33.5
CTLA4+
1.45
TIM3+
0.69
LAG3+
0.55

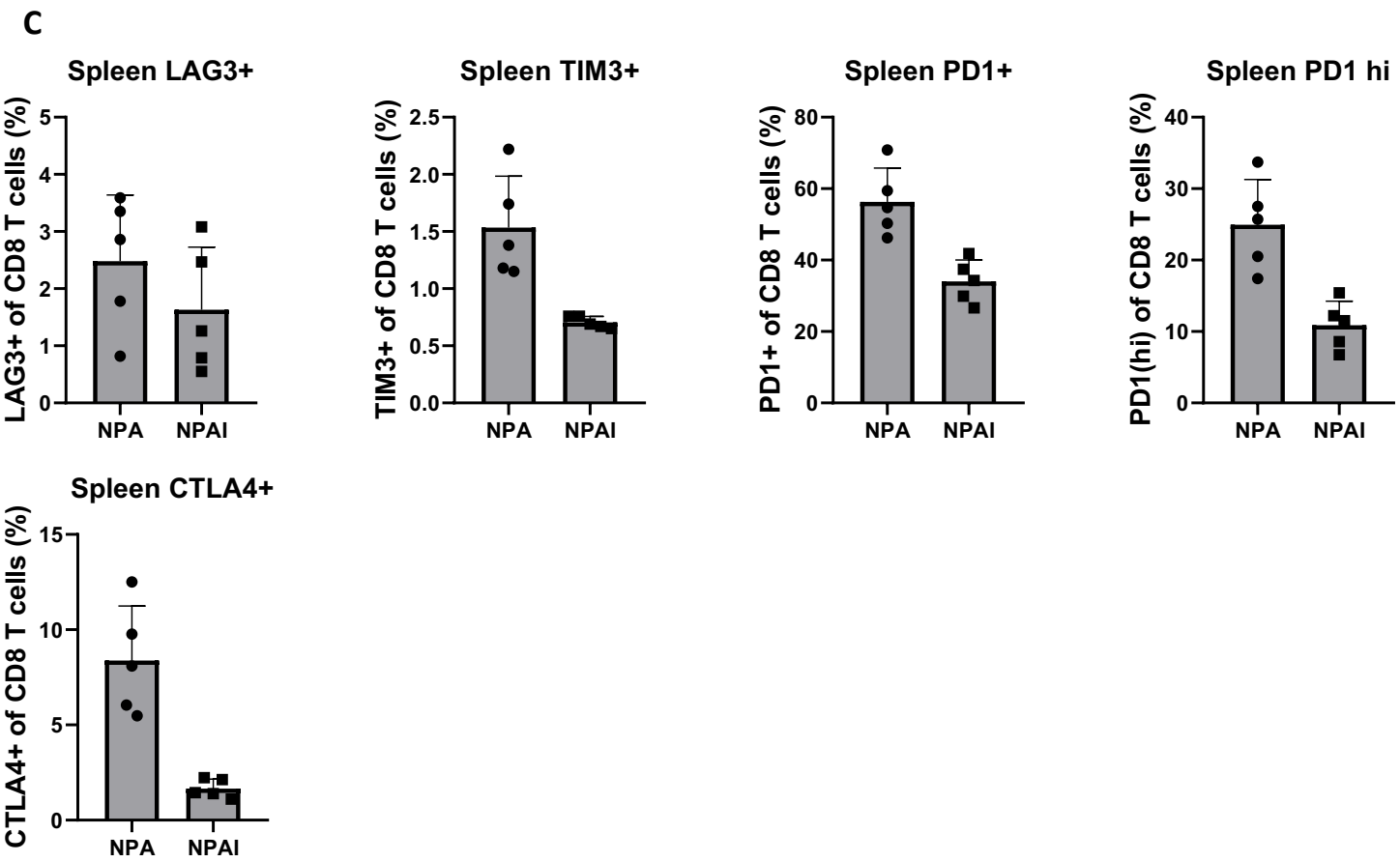

Figure 8: Data collected of spleen for CD8+ TIL exhaustion markers induced by mtIDH1. **(A)** and **(B)** represent the flow cytometry data of the NPAI and NPA model. **(C)** illustrates a graphical representation of the data.

Blood

There was a notable difference in the sample size between the two models. Analysis of the blood samples showed a significant difference in live immune cells found in the NPAI model compared to the NPA model. In the NPA model only 13.7% of the cells were live CD45+ cells, while in the NPAI model 54.3% of the sample was live CD45+ (shown in Figure 9.A and 9.B). Of the live immune cells detected, we are using a CD3 antibody to identify our T cell population. The NPA model showed a greater frequency of T cells compared to that of the NPAI model. The NPA model identified 17.6% of the population to be T cells, while the NPAI model identified 34.8% of the population to be T cells (shown in Figure 9.A and 9.B). From here, CD4 and CD8 antibodies were used to identify our helper T cells and cytotoxic T cells, respectively. The CD4+ population showed a greater frequency in the NPAI model than in the NPA model, with 31.7% compared to 18.5%, respectively (shown in Figure 9.A and 9.B). Our CD8+ populations however demonstrated a greater frequency in the NPA model than the NPAI model. The NPA model showed 44.4% of the T cell population to CD8+, while 29.9% of the NPAI T cell population were only considered CD8+ (shown in Figure 9.A and 9.B). Using the identified CD8+ population we continue investigating possible exhaustion markers on CD8+ T cells. As done in prior tissue samples, identification of PD-1 expression was noted by three population, PD-1 total, intermediate expression of PD-1, and high expression of PD-1. Of the two models, NPAI showed a greater overall PD-1 expression in total with a 46.1% frequency compared to 36.3% frequency in the NPA model (shown in Figure 9.A and 9.B). The intermediate and high expressions of the NPAI and NPA models are 33.4% and 22.6%, and 13.5% and 12.5%, respectively (shown in Figure 9.A and 9.B). CTLA-4 expression of the two models were nearly identical with the NPA exhibiting a frequency of 15.4% and NPAI exhibiting 15.0%. TIM-3 expression showed a significant difference expression in the NPA model compared to the NPAI. The CD8+ T cells of the NPA

model displayed 28.3% frequency, while the NPAI model displayed only a frequency of 4.79% (shown in Figure 9.A and 9.B). LAG-3 had the lowest expression of the possible exhaustion markers in the NPA and the NPAI model. In the NPA model, 2.46% of the identified CD8+ T cells expressed LAG-3, while the NPAI model showed an expression frequency of 3.99% (shown in Figure 9.A and 9.B).

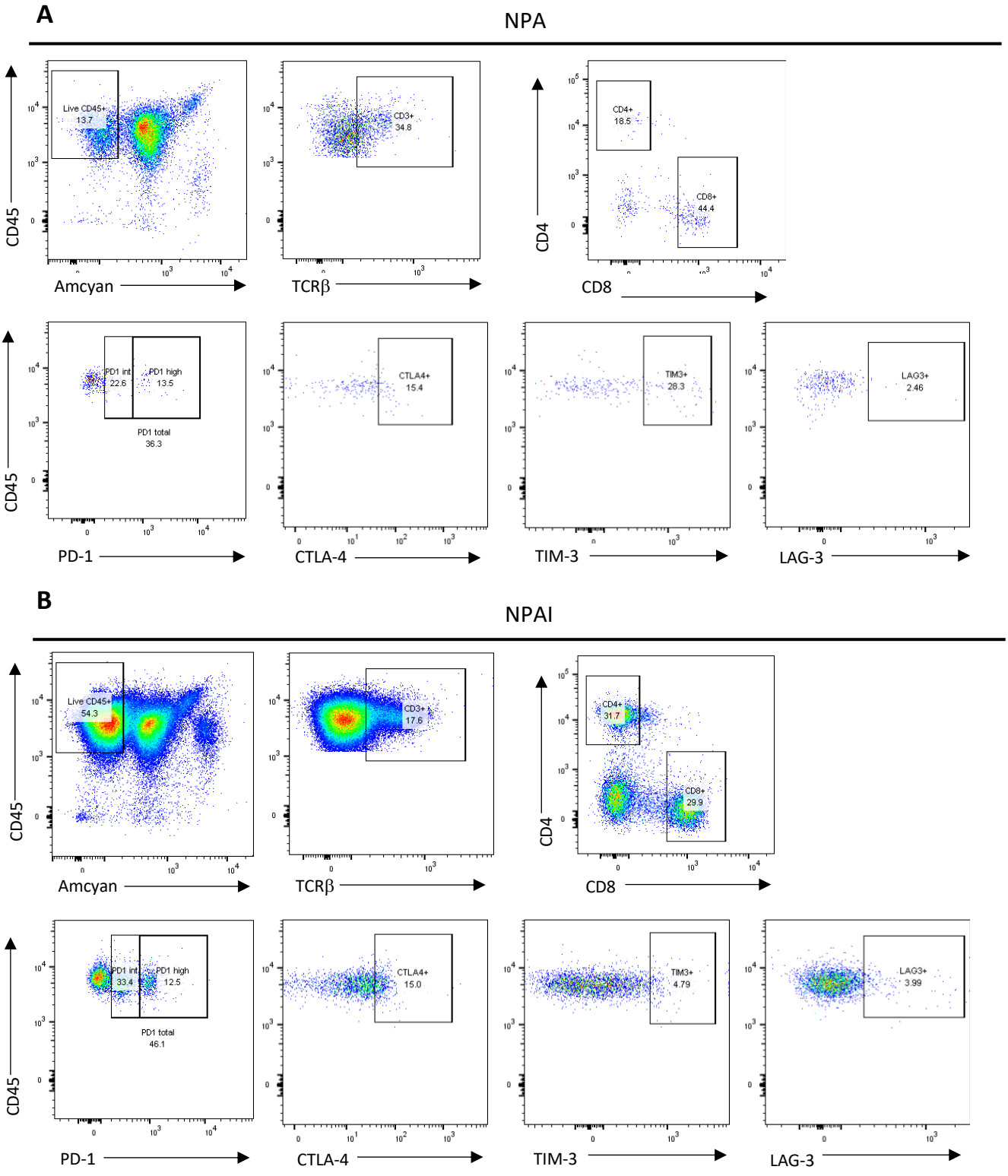
A
NPA
Live CD45+
13.7
CD3+
34.8
CD4+
18.5
CD8+
44.4
CD45
Amcyan
TCRβ
CD4
CD8
PD1 int
22.6
PD1 high
13.5
PD1 total
36.3
CTLA4+
15.4
TIM3+
28.3
LAG3+
2.46
PD-1
CTLA-4
TIM-3
LAG-3
B
NPAI
Live CD45+
54.3
CD3+
17.6
CD4+
31.7
CD8+
29.9
PD1 int
33.4
PD1 high
12.5
PD1 total
46.1
CTLA4+
15.0
TIM3+
4.79
LAG3+
3.99

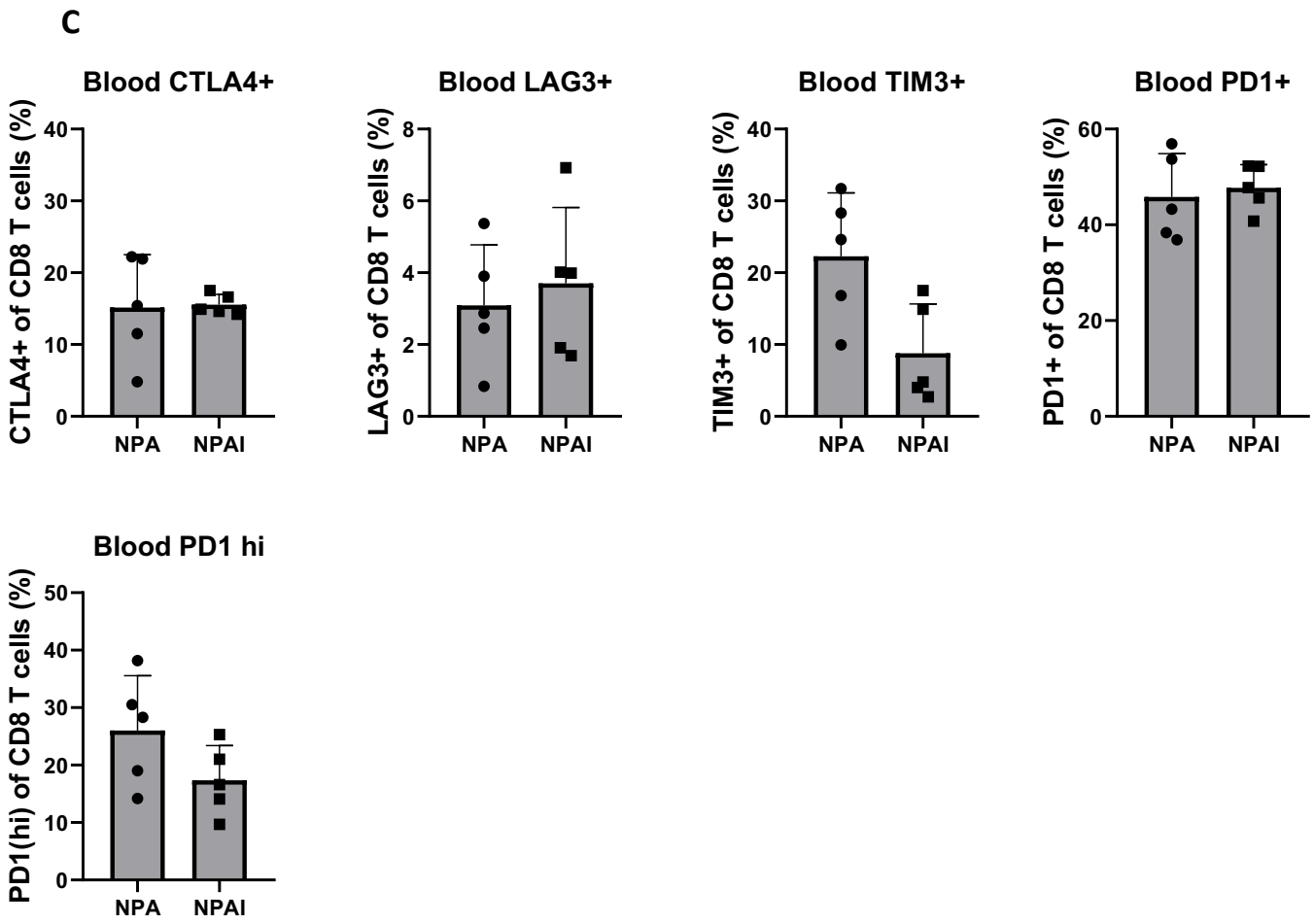

Figure 9: Data collected of blood for CD8+ TIL exhaustion markers induced by mtIDH1. **(A)** and **(B)** represent the flow cytometry data of the NPAI and NPA model. **(C)** illustrates a graphical representation of the data.

Survival Timeline with ICI Treatment

A survival experiment was established with three groups of mice: an NPA/NPAI control, an NPA with ICI treatment, and an NPAI with ICI treatment. After allowing a 7-day period for tumor development to progress, immune checkpoint inhibitors (ICI) or a control treatment of saline is given as an intraperitoneal injection in 200 microgram doses. Injections were given at day 7, 10, and 13. ICI treatment include anti-PD-1, anti-CTLA-4, anti-LAG-3, and anti-TIM-3. Tumor progression was visualized using IVIS imaging weekly through the process until endpoint is reached. Once the endpoint is reached the mice were perfused and the liver, brain, spleen, spinal cord, and blood were collected for possible future analysis.

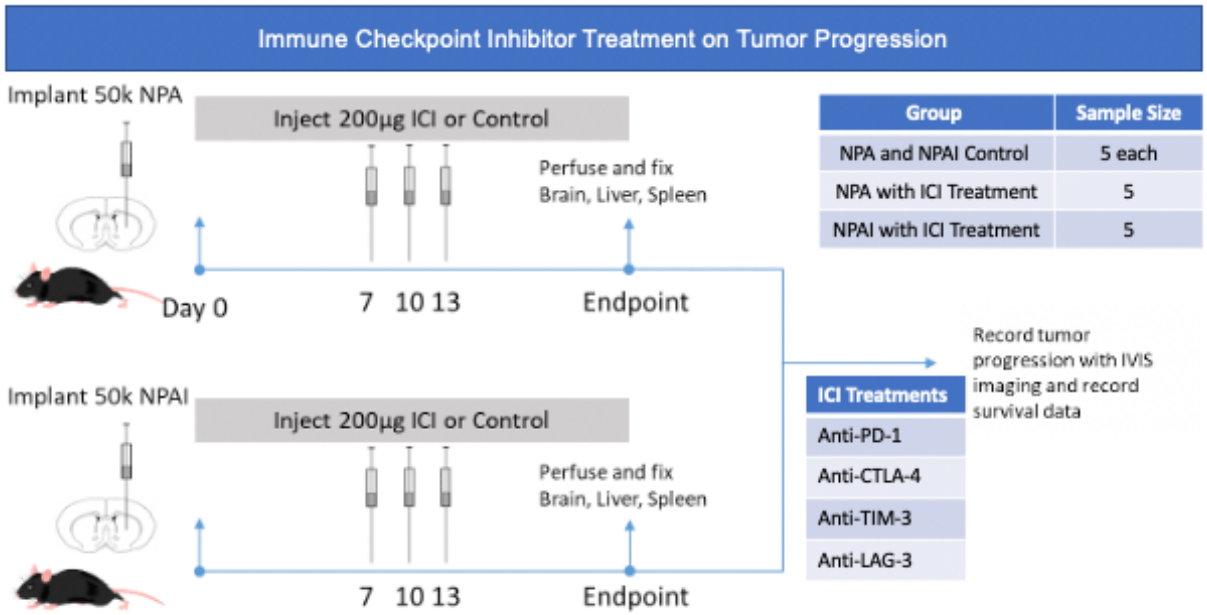

Figure 10: Experimental design of immune checkpoint inhibitor treatment. Mice were implanted with NPA or NPAI neurospheres and were even treated as a control or given ICI Treatments. Treatments were given day 7,10, and 13 post implantation. Once endpoint was reached the mice were euthanized, perfused, and the brain, liver, and spleen were fixed. IVIS imaging was taken to record tumor progression and changes with ICI treatments.

The first set of ICI treatments were completed using anti-PD-1 and anti-CTLA-4 ICIs. Four weeks' worth of imaging was recorded, shown in Figure 11. Using IVIS imaging software, the

region of interest was measured in terms of photons until they reached endpoint. The second set of ICI treatments were completed using anti-TIM-3 and LAG-3 ICIs. NPAI models responded well the ICI treatments, showing a greater survival time compared to their corresponding control groups. The median survival of the NPAI control of the TIM-3 and LAG-3 ICI treatment experiments was approximately only 40 days. The groups received the TIM-3 and LAG-3 ICI treatments have a median survival of at least 61 days. The NPAI control models of the PD-1 and CTLA-4 experiment had a median survival of 28 days while those that were given the treatment survived longer. However, in the NPA model some of the control mice survived longer than those that received PD-1 or CTLA-4 ICI treatments.

A NPAI – Control versus PD-1

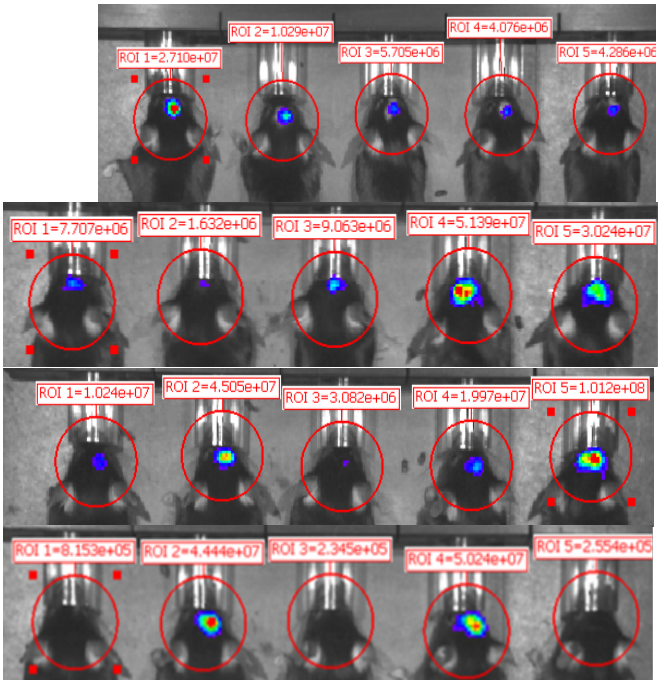

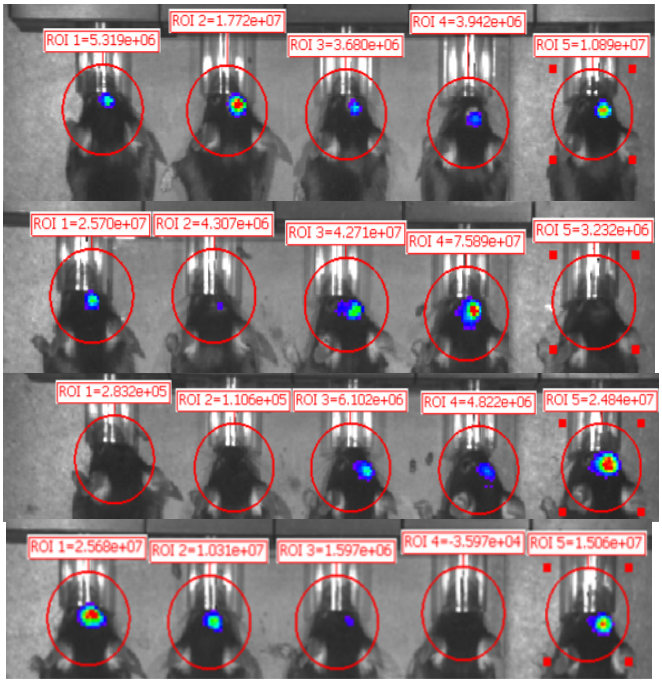

B NPA – Control versus PD-1

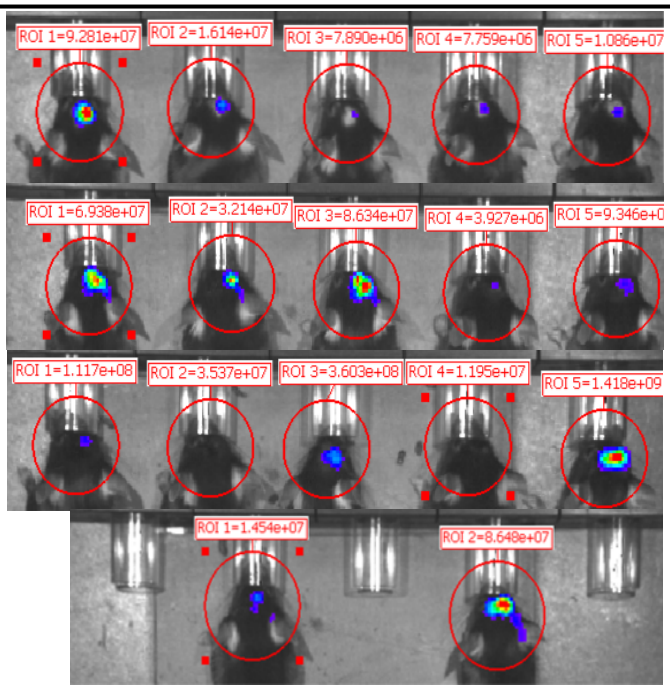

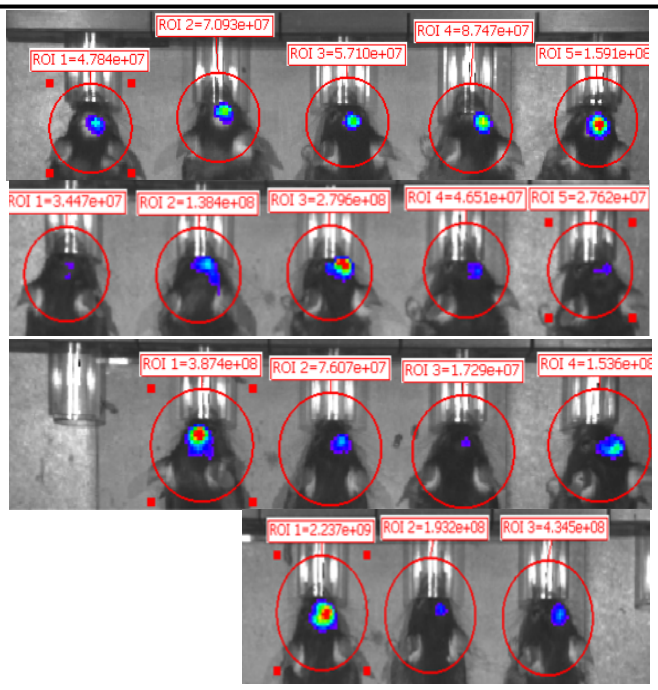

C

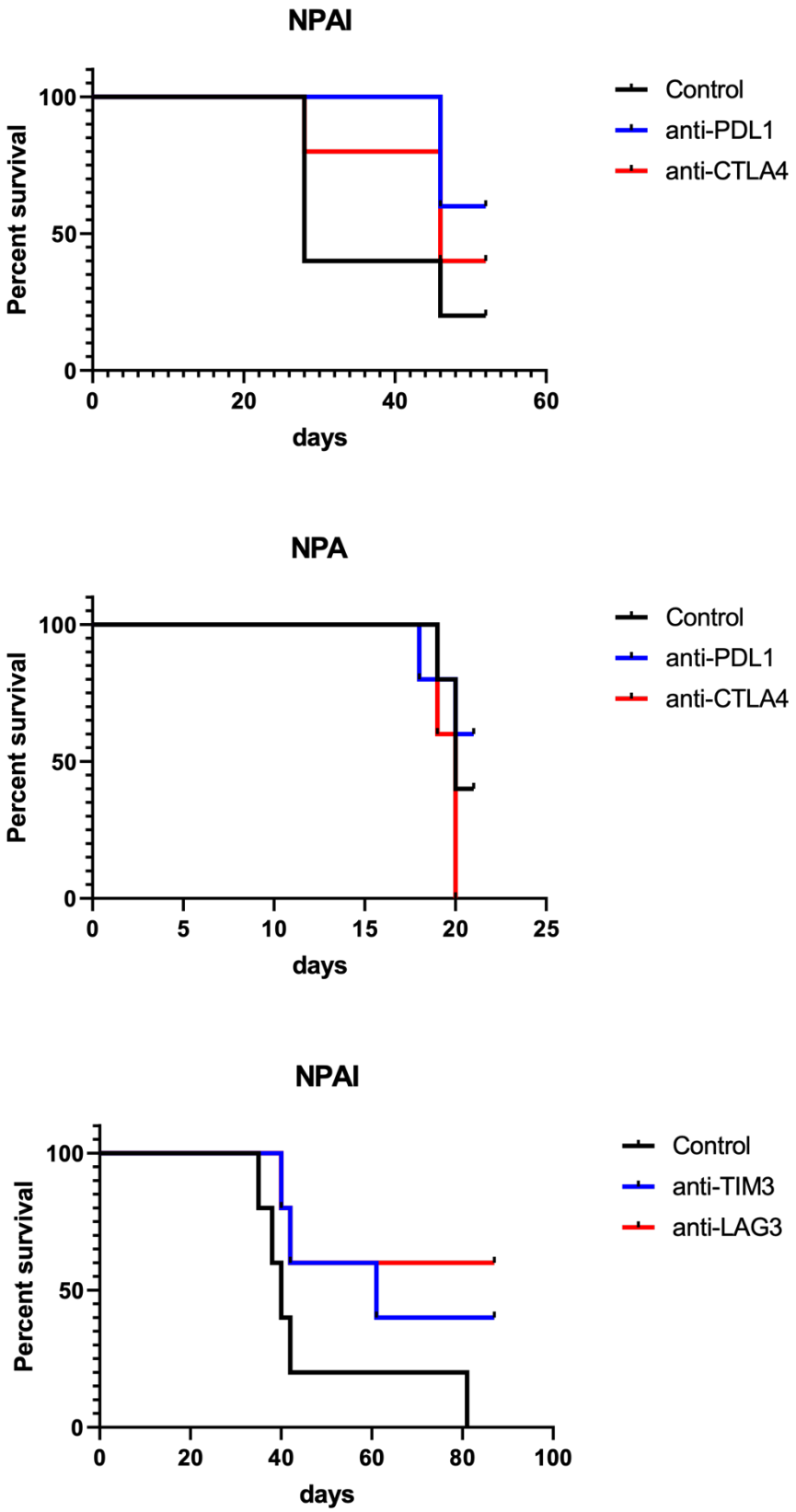

Figure 11: **(A)** and **(B)** show IVIS images collected of tumor progression in NPA and NPAI with and without anti-PD-1 treatment. **(C)** demonstrates survival curves of the mice versus their respective control groups.

Discussion

Exhaustion Markers Expression Analysis

The data collected for the identification of the exhaustion markers was not optimal. Due to having suboptimal populations of live CD45+ cells we limit the amount of T cells that we can acquire from this population. Even further this limits population size of our cytotoxic T cells which is critical in order to accurately quantify expression levels of possible exhaustion markers. Further assessments are being made into the protocol of obtaining the single cell suspension, specifically of the brain, to maintain a sufficient cell population.

In terms of the tumor microenvironment, we did observe a greater infiltration of immune cells within the brain of mice implanted with the NPA neurospheres compared to those implanted with NPAI. This is related to degree of deterioration present of the BBB found in wtIDH1 versus mtIDH1. The notable survival time in mtIDH1 may be affiliated with the preservation of the BBB limiting the infiltration of immune cells that are hijacked by the tumor microenvironment into an immunosuppressive nature. Notable remarks were found in possible exhaustion markers PD-1, TIM-3, and LAG-3. PD-1 displayed similar frequencies of expression across both NPA and NPAI models, leaving it difficult to discern from this data as to whether it is a cause for T cell exhaustion, aside from the data presented in other studies. The cell expression count did show statistical difference between the two however due to the variability and difference of live CD45+ cells collected this may be confounding issue. Increase in the NPAI model for TIM-3 expression showed statistical significance compared to that of the NPA. LAG-3 also showed an increase in expression in the NPAI model compared to the NPA however no statistical significance can be shown. The increase in TIM-3 and LAG-3 expression cannot be definitely tied to T cell exhaustion with the data we have present. An adjustment that is being made for further experiments is to suspend and

filter the tumor into accutase in order to clean the debris and break down the cells. This adjustment has shown better results in terms of viability.

The lymph nodes showed 60-70% frequency of live immune cells provided within the sample. The PD-1 expression was divided into identifying intermediate and high expression. This is due to the fact the T cell exhaustion was particularly identified at specific increased levels in PD-1 receptors. Lymph nodes of NPA mice showed a higher frequency of PD-1 receptors in total however, high expression of PD-1 was greater in the NPAI model. CTLA-4, TIM-3, and LAG-3 expressions are all less than 1% in frequency. The blood and spleen showed little to no difference in data in terms of expression of either PD-1, CTLA-4, TIM-3, or LAG-3.

ICI Treatment Survival Analysis

ICI treatments showed better results in the NPAI model compared to those shown in the NPA models. This can be attributed to the initial difference in survival time between the two models, in that the NPA model is more aggressive. Tumor development are at different phases in the NPA and NPAI models when ICI treatments are introduced, reducing the efficacy of the treatment in the NPA group. To account for this future experiments will begin ICI treatment within 2-3 days of implantation in both groups. Starting earlier treatment with ICI will hopefully change the prognosis on the survival time of the mice in more aggressive NPA models.

Conclusion

Development in molecular characterization and epigenomics has paved new insight onto identifying and analyzing mtIDH1, elicited heavily by 2-HG mediated inhibition. Understanding details such as these and the pathways that they are involved with provide further detail into investigating new approaches to current immunotherapies, as well as development of new immunotherapeutic techniques. Our current data demonstrates that the use of immune checkpoint

inhibitors does show efficacy in the advancing the median survival time of mice with implanted with NPAI neurospheres, however no direct result can be made as to whether this was related to depleting the development of exhausted T cells or promoting them into a terminal state towards apoptosis. Human trials are being conducting with the use of ICI treatments involving PD-1, CTLA-4, LAG-3, and TIM-3 (individually and in combination). A new approach as to looking at the state of exhausted T cells is to transition into looking at the ligands correlated to this receptors, for example PD-1/PDL-1, TIM-3/Gal9, and TIGIT/CD96. Investigation from this point of view may provide us with more detail on the pathway and better piece together the information from the two studies to draw upon a stronger conclusion from the results.

References

1. Ostrom, Q. T., Cioffi, G., Gittleman, H., Patil, N., Waite, K., Kruchko, C., & Barnholtz-Sloan, J. S. (2019). CBTRUS statistical report: Primary Brain and other central nervous system tumors diagnosed in the United States in 2012–2016. *Neuro-Oncology*, *21*(Supplement_5), v1–v100. https://doi.org/10.1093/neuonc/noz150[iii]

2. Louis, D. N., Perry, A., Reifenberger, G., von Deimling, A., Figarella-Branger, D., Cavenee, W. K., Ohgaki, H., Wiestler, O. D., Kleihues, P., & Ellison, D. W. (2016). The 2016 world Health Organization classification of tumors of the central nervous system: A summary. *Acta Neuropathologica*, *131*(6), 803–820. https://doi.org/10.1007/s00401-016-1545-1

3. Schiff, D., Brown, P. D., & Giannini, C. (2007). Outcome in adult low-grade glioma: The impact of prognostic factors and treatment. *Neurology*, *69*(13), 1366–1373. https://doi.org/10.1212/01.wnl.0000277271.47601.a1

4. Waitkus, M. S., Diplas, B. H., & Yan, H. (2015). Isocitrate dehydrogenase mutations in gliomas. *Neuro-Oncology*, *18*(1), 16–26. https://doi.org/10.1093/neuonc/nov136

5. Walker, P. R., Prins, R. M., Dietrich, P.-Y., & Liau, L. M. (2009). Harnessing T-cell immunity to target brain tumors. *CNS Cancer*, 1165–1217. https://doi.org/10.1007/978-1-60327-553-8_48

6. Alghamri, M. S., McClellan, B. L., Avvari, R. P., Thalla, R., Carney, S., Hartlage, M. S., Haase, S., Ventosa, M., Taher, A., Kamran, N., Zhang, L., Faisal, S. M., Núñez, F. J., Garcia-Fabiani, M. B., Al-Holou, W. N., Orringer, D., Hervey-Jumper, S., Heth, J., Patil, P. G., … Castro, M. G. (2021). G-CSF secreted by mutant Idh1 glioma stem cells abolishes myeloid cell immunosuppression and enhances the efficacy of immunotherapy. *Science Advances*, *7*(40). https://doi.org/10.1126/sciadv.abh3243

7. Forst, D. A., Nahed, B. V., Loeffler, J. S., & Batchelor, T. T. (2014). Low-grade gliomas. *The Oncologist*, *19*(4), 403–413. https://doi.org/10.1634/theoncologist.2013-0345

8. Brown, T. J., Bota, D. A., van Den Bent, M. J., Brown, P. D., Maher, E., Aregawi, D., Liau, L. M., Buckner, J. C., Weller, M., Berger, M. S., & Glantz, M. (2018). Management of low-grade glioma: A systematic review and meta-analysis. *Neuro-Oncology Practice*, *6*(4), 249–258. https://doi.org/10.1093/nop/npy034

9. Louis, D. N., Perry, A., Wesseling, P., Brat, D. J., Cree, I. A., Figarella-Branger, D., Hawkins, C., Ng, H. K., Pfister, S. M., Reifenberger, G., Soffietti, R., von Deimling, A., & Ellison, D. W. (2021). The 2021 who classification of tumors of the central nervous system: A summary. *Neuro-Oncology*, *23*(8), 1231–1251. https://doi.org/10.1093/neuonc/noab106

10. Han, S., Liu, Y., Cai, S. J., Qian, M., Ding, J., Larion, M., Gilbert, M. R., & Yang, C. (2020). IDH mutation in glioma: Molecular mechanisms and potential therapeutic targets. *British Journal of Cancer*, *122*(11), 1580–1589. https://doi.org/10.1038/s41416-020-0814-x

11. Uhm, J. (2009). IDH1 and IDH2 mutations in gliomas. *Yearbook of Neurology and Neurosurgery*, *2009*, 119–120. https://doi.org/10.1016/s0513-5117(09)79085-4

12. Ceccarelli, M., Barthel, F. P., Malta, T. M., Sabedot, T. S., Salama, S. R., Murray, B. A., Morozova, O., Newton, Y., Radenbaugh, A., Pagnotta, S. M., Anjum, S., Wang, J., Manyam, G., Zoppoli, P., Ling, S., Rao, A. A., Grifford, M., Cherniack, A. D., Zhang, H., … Zmuda, E. (2016). Molecular profiling reveals biologically discrete subsets and pathways of progression in diffuse glioma. *Cell*, *164*(3), 550–563. https://doi.org/10.1016/j.cell.2015.12.028

13. Chen, R., Smith-Cohn, M., Cohen, A. L., & Colman, H. (2017). Glioma subclassifications and their clinical significance. *Neurotherapeutics*, *14*(2), 284–297. https://doi.org/10.1007/s13311-017-0519-x

14. Xu, X., Zhao, J., Xu, Z., Peng, B., Huang, Q., Arnold, E., & Ding, J. (2004). Structures of human cytosolic NADP-dependent isocitrate dehydrogenase reveal a novel self-regulatory mechanism of activity. *Journal of Biological Chemistry*, *279*(32), 33946–33957. https://doi.org/10.1074/jbc.m404298200

15. Kim, Y.-O., Koh, H.-J., Kim, S.-H., Jo, S.-H., Huh, J.-W., Jeong, K.-S., Lee, I. J., Song, B. J., & Huh, T.-L. (1999). Identification and functional characterization of a novel, tissue-specific nad+-dependent isocitrate dehydrogenase β subunit isoform. *Journal of Biological Chemistry*, *274*(52), 36866–36875. https://doi.org/10.1074/jbc.274.52.36866

16. Al-Khallaf, H. (2017). Isocitrate dehydrogenases in physiology and cancer: Biochemical and molecular insight. *Cell & Bioscience*, *7*(1). https://doi.org/10.1186/s13578-017-0165-3

17. DICKINSON, D. A. L. E. A., & FORMAN, H. E. N. R. Y. J. A. Y. (2002). Glutathione in defense and Signaling. *Annals of the New York Academy of Sciences*, *973*(1), 488–504. https://doi.org/10.1111/j.1749-6632.2002.tb04690.x

18. Avery, A. M., Willetts, S. A., & Avery, S. V. (2004). Genetic dissection of the phospholipid hydroperoxidase activity of yeast Gpx3 reveals its functional importance. *Journal of Biological Chemistry*, *279*(45), 46652–46658. https://doi.org/10.1074/jbc.m408340200

19. Mycielska, M. E., Patel, A., Rizaner, N., Mazurek, M. P., Keun, H., Patel, A., Ganapathy, V., & Djamgoz, M. B. (2009). Citrate transport and metabolism in mammalian cells. *BioEssays*, *31*(1), 10–20. https://doi.org/10.1002/bies.080137

20. Dang, L., Yen, K., & Attar, E. C. (2016). IDH mutations in cancer and progress toward development of Targeted Therapeutics. *Annals of Oncology*, *27*(4), 599–608. https://doi.org/10.1093/annonc/mdw013

21. Kang, M. R., Kim, M. S., Oh, J. E., Kim, Y. R., Song, S. Y., Seo, S. I., Lee, J. Y., Yoo, N. J., & Lee, S. H. (2009). Mutational analysis of IDH1 codon 132 in glioblastomas and other common cancers. *International Journal of Cancer*, *125*(2), 353–355. https://doi.org/10.1002/ijc.24379

22. Waitkus, M. S., Diplas, B. H., & Yan, H. (2018). Biological role and therapeutic potential of IDH mutations in cancer. *Cancer Cell*, *34*(2), 186–195. https://doi.org/10.1016/j.ccell.2018.04.011

23. Yan, H., Parsons, D. W., Jin, G., McLendon, R., Rasheed, B. A., Yuan, W., Kos, I., Batinic-Haberle, I., Jones, S., Riggins, G. J., Friedman, H., Friedman, A., Reardon, D., Herndon, J., Kinzler, K. W., Velculescu, V. E., Vogelstein, B., & Bigner, D. D. (2009). IDH1andIDH2Mutations in gliomas. *New England Journal of Medicine*, *360*(8), 765–773. https://doi.org/10.1056/nejmoa0808710

24. Medeiros, B. C., Fathi, A. T., DiNardo, C. D., Pollyea, D. A., Chan, S. M., & Swords, R. (2016). Isocitrate dehydrogenase mutations in myeloid malignancies. *Leukemia*, *31*(2), 272–281. https://doi.org/10.1038/leu.2016.275

25. Dang, L., White, D. W., Gross, S., Bennett, B. D., Bittinger, M. A., Driggers, E. M., Fantin, V. R., Jang, H. G., Jin, S., Keenan, M. C., Marks, K. M., Prins, R. M., Ward, P. S., Yen, K. E., Liau, L. M., Rabinowitz, J. D., Cantley, L. C., Thompson, C. B., Vander Heiden, M. G., & Su, S. M. (2009). Cancer-associated IDH1 mutations produce 2-hydroxyglutarate. *Nature*, *462*(7274), 739–744. https://doi.org/10.1038/nature08617

26. Elkhaled, A., Jalbert, L. E., Phillips, J. J., Yoshihara, H. A., Parvataneni, R., Srinivasan, R., Bourne, G., Berger, M. S., Chang, S. M., Cha, S., & Nelson, S. J. (2012). Magnetic resonance of 2-hydroxyglutarate in Idh1 -mutated low-grade gliomas. *Science Translational Medicine*, *4*(116). https://doi.org/10.1126/scitranslmed.3002796

27. Tommasini-Ghelfi, S., Murnan, K., Kouri, F. M., Mahajan, A. S., May, J. L., & Stegh, A. H. (2019). Cancer-associated mutation and beyond: The emerging biology of isocitrate dehydrogenases in human disease. *Science Advances*, *5*(5). https://doi.org/10.1126/sciadv.aaw4543

28. Xu, W., Yang, H., Liu, Y., Yang, Y., Wang, P., Kim, S.-H., Ito, S., Yang, C., Wang, P., Xiao, M.-T., Liu, L.-xia, Jiang, W.-qing, Liu, J., Zhang, J.-ye, Wang, B., Frye, S., Zhang, Y., Xu, Y.-hui, Lei, Q.-ying, … Xiong, Y. (2011). Oncometabolite 2-hydroxyglutarate is a competitive inhibitor of α-ketoglutarate-dependent dioxygenases. *Cancer Cell*, *19*(1), 17–30. https://doi.org/10.1016/j.ccr.2010.12.014

29. Chou, F.-J., Liu, Y., Lang, F., & Yang, C. (2021). D-2-hydroxyglutarate in Glioma Biology. *Cells*, *10*(9), 2345. https://doi.org/10.3390/cells10092345

30. Jones, P. A., & Baylin, S. B. (2007). The epigenomics of cancer. *Cell*, *128*(4), 683–692. https://doi.org/10.1016/j.cell.2007.01.029

31. Hermann, A., Goyal, R., & Jeltsch, A. (2004). The dnmt1 dna-(cytosine-c5)-methyltransferase methylates DNA processively with high preference for hemimethylated target sites. *Journal of Biological Chemistry*, *279*(46), 48350–48359. https://doi.org/10.1074/jbc.m403427200

32. Okano, M., Bell, D. W., Haber, D. A., & Li, E. (1999). DNA methyltransferases dnmt3a and dnmt3b are essential for de novo methylation and mammalian development. *Cell*, *99*(3), 247–257. https://doi.org/10.1016/s0092-8674(00)81656-6

33. Liu, Y., Jiang, W., Liu, J., Zhao, S., Xiong, J., Mao, Y., & Wang, Y. (2012). IDH1 mutations inhibit multiple α-ketoglutarate-dependent dioxygenase activities in astroglioma. *Journal of Neuro-Oncology*, *109*(2), 253–260. https://doi.org/10.1007/s11060-012-0914-4

34. Ehrlich, M. (2019). DNA hypermethylation in disease: Mechanisms and clinical relevance. *Epigenetics*, *14*(12), 1141–1163. https://doi.org/10.1080/15592294.2019.1638701

35. Duncan, C. G., Barwick, B. G., Jin, G., Rago, C., Kapoor-Vazirani, P., Powell, D. R., Chi, J.-T., Bigner, D. D., Vertino, P. M., & Yan, H. (2012). A heterozygous IDH1R132H/WT mutation induces genome-wide alterations in DNA methylation. *Genome Research*, *22*(12), 2339–2355. https://doi.org/10.1101/gr.132738.111

36. Noushmehr, H., Weisenberger, D. J., Diefes, K., Phillips, H. S., Pujara, K., Berman, B. P., Pan, F., Pelloski, C. E., Sulman, E. P., Bhat, K. P., Verhaak, R. G. W., Hoadley, K. A., Hayes, D. N., Perou, C. M., Schmidt, H. K., Ding, L., Wilson, R. K., Van Den Berg, D., Shen, H., … Aldape, K. (2010). Identification of a CPG island methylator phenotype that defines a distinct subgroup of glioma. *Cancer Cell*, *17*(5), 510–522. https://doi.org/10.1016/j.ccr.2010.03.017

37. Christensen, B. C., Smith, A. A., Zheng, S., Koestler, D. C., Houseman, E. A., Marsit, C. J., Wiemels, J. L., Nelson, H. H., Karagas, M. R., Wrensch, M. R., Kelsey, K. T., & Wiencke, J. K. (2011). DNA methylation, isocitrate dehydrogenase mutation, and survival in glioma. *JNCI: Journal of the National Cancer Institute*, *103*(2), 143–153. https://doi.org/10.1093/jnci/djq497

38. Turcan, S., Rohle, D., Goenka, A., Walsh, L. A., Fang, F., Yilmaz, E., Campos, C., Fabius, A. W., Lu, C., Ward, P. S., Thompson, C. B., Kaufman, A., Guryanova, O., Levine, R., Heguy, A., Viale, A., Morris, L. G., Huse, J. T., Mellinghoff, I. K., & Chan, T. A. (2012). IDH1 mutation is sufficient to establish the glioma hypermethylator phenotype. *Nature*, *483*(7390), 479–483. https://doi.org/10.1038/nature10866

39. Sasaki, M., Knobbe, C. B., Itsumi, M., Elia, A. J., Harris, I. S., Chio, I. I., Cairns, R. A., McCracken, S., Wakeham, A., Haight, J., Ten, A. Y., Snow, B., Ueda, T., Inoue, S., Yamamoto, K., Ko, M., Rao, A., Yen, K. E., Su, S. M., & Mak, T. W. (2012). D-2-hydroxyglutarate produced by mutant IDH1 perturbs collagen maturation and basement membrane function. *Genes & Development*, *26*(18), 2038–2049. https://doi.org/10.1101/gad.198200.112

40. Bardella, C., Al-Dalahmah, O., Krell, D., Brazauskas, P., Al-Qahtani, K., Tomkova, M., Adam, J., Serres, S., Lockstone, H., Freeman-Mills, L., Pfeffer, I., Sibson, N., Goldin, R., Schuster-Böeckler, B., Pollard, P. J., Soga, T., McCullagh, J. S., Schofield, C. J., Mulholland, P., … Tomlinson, I. (2016). Expression of idh1r132h in the murine subventricular zone stem cell niche recapitulates features of early gliomagenesis. *Cancer Cell*, *30*(4), 578–594. https://doi.org/10.1016/j.ccell.2016.08.017

41. Bettegowda, C., Agrawal, N., Jiao, Y., Sausen, M., Wood, L. D., Hruban, R. H., Rodriguez, F. J., Cahill, D. P., McLendon, R., Riggins, G., Velculescu, V. E., Oba-Shinjo, S. M., Marie, S. K., Vogelstein, B., Bigner, D., Yan, H., Papadopoulos, N., & Kinzler, K. W. (2011). Mutations in CIC and FUBP1 contribute to human oligodendroglioma. *Science*, *333*(6048), 1453–1455. https://doi.org/10.1126/science.1210557

42. Jiao, Y., Killela, P. J., Reitman, Z. J., Rasheed, B. A., Heaphy, C. M., de Wilde, R. F., Rodriguez, F. J., Rosemberg, S., Oba-Shinjo, S. M., Nagahashi Marie, S. K., Bettegowda, C., Agrawal, N., Lipp, E., Pirozzi, C. J., Lopez, G. Y., He, Y., Friedman, H. S., Friedman, A. H., Riggins, G. J., … Yan, H. (2012). Frequent ATRX, CIC, FUBP1 and IDH1 mutations refine the classification of malignant gliomas. *Oncotarget*, *3*(7), 709–722. https://doi.org/10.18632/oncotarget.588

43. Tsukada, Y.-ichi, Fang, J., Erdjument-Bromage, H., Warren, M. E., Borchers, C. H., Tempst, P., & Zhang, Y. (2005). Histone demethylation by a family of jmjc domain-containing proteins. *Nature*, *439*(7078), 811–816. https://doi.org/10.1038/nature04433

44. Höpfl, G., Ogunshola, O., & Gassmann, M. (2004). HIFs and tumors—causes and consequences. *American Journal of Physiology-Regulatory, Integrative and Comparative Physiology*, *286*(4). https://doi.org/10.1152/ajpregu.00538.2003

45. Berger, S. L. (2007). The complex language of chromatin regulation during transcription. *Nature*, *447*(7143), 407–412. https://doi.org/10.1038/nature05915

46. Barski, A., Cuddapah, S., Cui, K., Roh, T.-Y., Schones, D. E., Wang, Z., Wei, G., Chepelev, I., & Zhao, K. (2007). High-resolution profiling of histone methylations in the human genome. *Cell*, *129*(4), 823–837. https://doi.org/10.1016/j.cell.2007.05.009

47. Lu, C., Ward, P. S., Kapoor, G. S., Rohle, D., Turcan, S., Abdel-Wahab, O., Edwards, C. R., Khanin, R., Figueroa, M. E., Melnick, A., Wellen, K. E., O'Rourke, D. M., Berger, S. L., Chan, T. A., Levine, R. L., Mellinghoff, I. K., & Thompson, C. B. (2012). IDH mutation impairs histone demethylation and results in a block to cell differentiation. *Nature*, *483*(7390), 474–478. https://doi.org/10.1038/nature10860

48. Chi, P., Allis, C. D., & Wang, G. G. (2010). Covalent histone modifications — miswritten, misinterpreted and mis-erased in human cancers. *Nature Reviews Cancer*, *10*(7), 457–469. https://doi.org/10.1038/nrc2876

49. Francisco, L. M., Salinas, V. H., Brown, K. E., Vanguri, V. K., Freeman, G. J., Kuchroo, V. K., & Sharpe, A. H. (2009). PD-L1 regulates the development, maintenance, and function of induced regulatory T cells. *Journal of Experimental Medicine*, *206*(13), 3015–3029. https://doi.org/10.1084/jem.20090847

50. Röver, L. K., Gevensleben, H., Dietrich, J., Bootz, F., Landsberg, J., Goltz, D., & Dietrich, D. (2018). PD-1 (PDCD1) promoter methylation is a prognostic factor in patients with diffuse lower-grade gliomas harboring isocitrate dehydrogenase (IDH) mutations. *EBioMedicine*, *28*, 97–104. https://doi.org/10.1016/j.ebiom.2018.01.016

51. Arvanitis, C. D., Ferraro, G. B., & Jain, R. K. (2019). The blood–brain barrier and blood–tumour barrier in brain tumours and metastases. *Nature Reviews Cancer*, *20*(1), 26–41. https://doi.org/10.1038/s41568-019-0205-x

52. Quail, D. F., & Joyce, J. A. (2017). The microenvironmental landscape of brain tumors. *Cancer Cell*, *31*(3), 326–341. https://doi.org/10.1016/j.ccell.2017.02.009

53. Varatharaj, A., & Galea, I. (2017). The blood-brain barrier in systemic inflammation. *Brain, Behavior, and Immunity*, *60*, 1–12. https://doi.org/10.1016/j.bbi.2016.03.010

54. Da Ros, M., De Gregorio, V., Iorio, A., Giunti, L., Guidi, M., de Martino, M., Genitori, L., & Sardi, I. (2018). Glioblastoma chemoresistance: The double play by Microenvironment and blood-brain barrier. *International Journal of Molecular Sciences*, *19*(10), 2879. https://doi.org/10.3390/ijms19102879

55. Bergers, G., & Benjamin, L. E. (2003). Tumorigenesis and the Angiogenic Switch. *Nature Reviews Cancer*, *3*(6), 401–410. https://doi.org/10.1038/nrc1093

56. Sharma, H. S. (2009). Blood–central nervous system barriers: The gateway to neurodegeneration, neuroprotection and neuroregeneration. *Handbook of Neurochemistry and Molecular Neurobiology*, 363–457. https://doi.org/10.1007/978-0-387-30375-8_17

57. Erickson, M. A., Dohi, K., & Banks, W. A. (2012). Neuroinflammation: A common pathway in CNS diseases as mediated at the blood-brain barrier. *Neuroimmunomodulation*, *19*(2), 121–130. https://doi.org/10.1159/000330247

58. Allavena, P., Sica, A., Solinas, G., Porta, C., & Mantovani, A. (2008). The inflammatory micro-environment in tumor progression: The role of tumor-associated macrophages. *Critical Reviews in Oncology/Hematology*, *66*(1), 1–9. https://doi.org/10.1016/j.critrevonc.2007.07.004

59. Kaur, B., Khwaja, F. W., Severson, E. A., Matheny, S. L., Brat, D. J., & Van Meir, E. G. (2005). Hypoxia and the hypoxia-inducible-factor pathway in glioma growth andangiogenesis. *Neuro-Oncology*, *7*(2), 134–153. https://doi.org/10.1215/s1152851704001115

60. Murat, A., Migliavacca, E., Hussain, S. F., Heimberger, A. B., Desbaillets, I., Hamou, M.-F., Rüegg, C., Stupp, R., Delorenzi, M., & Hegi, M. E. (2009). Modulation of angiogenic and inflammatory response in glioblastoma by hypoxia. *PLoS ONE*, *4*(6). https://doi.org/10.1371/journal.pone.0005947

61. Belykh, E., Shaffer, K. V., Lin, C., Byvaltsev, V. A., Preul, M. C., & Chen, L. (2020). Blood-brain barrier, blood-brain tumor barrier, and fluorescence-guided neurosurgical oncology: Delivering optical labels to brain tumors. *Frontiers in Oncology*, *10*. https://doi.org/10.3389/fonc.2020.00739

62. Dubois, L. G., Campanati, L., Righy, C., Dâ€™Andrea-Meira, I., Spohr, T. C., Porto-Carreiro, I., Pereira, C. M., BalÃ§a-Silva, J., Kahn, S. A., DosSantos, M. F., Oliveira, M. de, Ximenes-da-Silva, A., Lopes, M. C., Faveret, E., Gasparetto, E. L., & Moura-Neto, V. (2014). Gliomas and the vascular fragility of the Blood Brain Barrier. *Frontiers in Cellular Neuroscience*, *8*. https://doi.org/10.3389/fncel.2014.00418

63. Alghamri, M. S., McClellan, B. L., Hartlage, M. S., Haase, S., Faisal, S. M., Thalla, R., Dabaja, A., Banerjee, K., Carney, S. V., Mujeeb, A. A., Olin, M. R., Moon, J. J., Schwendeman, A., Lowenstein, P. R., & Castro, M. G. (2021). Targeting neuroinflammation in brain cancer: Uncovering mechanisms, pharmacological targets, and neuropharmaceutical developments. *Frontiers in Pharmacology*, *12*. https://doi.org/10.3389/fphar.2021.680021

64. Sonar, S. A., & Lal, G. (2018). Blood-brain barrier and its function during inflammation and autoimmunity. *Journal of Leukocyte Biology*, *103*(5), 839–853. https://doi.org/10.1002/jlb.1ru1117-428r

65. Sethi, G. (2008). TNF: A master switch for inflammation to cancer. *Frontiers in Bioscience*, *Volume*(13), 5094. https://doi.org/10.2741/3066

66. Kore, R. A., & Abraham, E. C. (2014). Inflammatory cytokines, interleukin-1 beta and tumor necrosis factor-alpha, upregulated in glioblastoma multiforme, raise the levels of Cryab in exosomes secreted by U373 glioma cells. *Biochemical and Biophysical Research Communications*, *453*(3), 326–331. https://doi.org/10.1016/j.bbrc.2014.09.068

67. Könnecke, H., & Bechmann, I. (2013). The role of microglia and matrix metalloproteinases involvement in neuroinflammation and gliomas. *Clinical and Developmental Immunology*, *2013*, 1–15. https://doi.org/10.1155/2013/914104

68. Joseph, J. V., Balasubramaniyan, V., Walenkamp, A., & Kruyt, F. A. E. (2013). TGF-β as a therapeutic target in high grade gliomas – promises and challenges. Biochemical Pharmacology, 85(4), 478–485. https://doi.org/10.1016/j.bcp.2012.11.005

69. Wolburg, H., Noell, S., Fallier-Becker, P., Mack, A. F., & Wolburg-Buchholz, K. (2012). The disturbed blood–brain barrier in human glioblastoma. *Molecular Aspects of Medicine*, *33*(5-6), 579–589. https://doi.org/10.1016/j.mam.2012.02.003

70. Zhou, W., Chen, C., Shi, Y., Wu, Q., Gimple, R. C., Fang, X., Huang, Z., Zhai, K., Ke, S. Q., Ping, Y.-F., Feng, H., Rich, J. N., Yu, J. S., Bao, S., & Bian, X.-W. (2017). Targeting glioma stem cell-derived pericytes disrupts the blood-tumor barrier and improves chemotherapeutic efficacy. *Cell Stem Cell*, *21*(5). https://doi.org/10.1016/j.stem.2017.10.002

71. Gieryng, A., Pszczolkowska, D., Walentynowicz, K. A., Rajan, W. D., & Kaminska, B. (2017). Immune microenvironment of gliomas. *Laboratory Investigation*, *97*(5), 498–518. https://doi.org/10.1038/labinvest.2017.19

72. Vasievich, E. A., & Huang, L. (2011). The suppressive tumor microenvironment: A challenge in cancer immunotherapy. *Molecular Pharmaceutics*, *8*(3), 635–641. https://doi.org/10.1021/mp1004228

73. Schetters, S. T., Gomez-Nicola, D., Garcia-Vallejo, J. J., & Van Kooyk, Y. (2018). Neuroinflammation: Microglia and T cells get ready to Tango. *Frontiers in Immunology*, *8*. https://doi.org/10.3389/fimmu.2017.01905

74. Russo, C. D., & Cappoli, N. (2018). Glioma associated microglia/macrophages, a potential pharmacological target to promote antitumor inflammatory immune response in the treatment of glioblastoma. *Neuroimmunology and Neuroinflammation*, *5*(9), 36. https://doi.org/10.20517/2347-8659.2018.42

75. Gutmann, D. H., & Kettenmann, H. (2019). Microglia/brain macrophages as central drivers of brain tumor pathobiology. *Neuron*, *104*(3), 442–449. https://doi.org/10.1016/j.neuron.2019.08.028

76. Hambardzumyan, D., Gutmann, D. H., & Kettenmann, H. (2015). The role of microglia and macrophages in glioma maintenance and progression. *Nature Neuroscience*, *19*(1), 20–27. https://doi.org/10.1038/nn.4185

77. Roesch, S., Rapp, C., Dettling, S., & Herold-Mende, C. (2018). When immune cells turn bad—tumor-associated microglia/macrophages in glioma. *International Journal of Molecular Sciences*, *19*(2), 436. https://doi.org/10.3390/ijms19020436

78. Zhang, J., Sarkar, S., Cua, R., Zhou, Y., Hader, W., & Yong, V. W. (2011). A dialog between glioma and microglia that promotes tumor invasiveness through the CCL2/ccr2/interleukin-6 axis. *Carcinogenesis*, *33*(2), 312–319. https://doi.org/10.1093/carcin/bgr289

79. Grabowski, M. M., Sankey, E. W., Ryan, K. J., Chongsathidkiet, P., Lorrey, S. J., Wilkinson, D. S., & Fecci, P. E. (2020). Immune suppression in gliomas. *Journal of Neuro-Oncology*, *151*(1), 3–12. https://doi.org/10.1007/s11060-020-03483-y

80. Mi, Y., Guo, N., Luan, J., Cheng, J., Hu, Z., Jiang, P., Jin, W., & Gao, X. (2020). The emerging role of myeloid-derived suppressor cells in the glioma immune suppressive microenvironment. *Frontiers in Immunology*, *11*. https://doi.org/10.3389/fimmu.2020.00737

81. Miyazaki, T., Ishikawa, E., Sugii, N., & Matsuda, M. (2020). Therapeutic strategies for overcoming immunotherapy resistance mediated by immunosuppressive factors of the glioblastoma microenvironment. *Cancers*, *12*(7), 1960. https://doi.org/10.3390/cancers12071960

82. Ostrand-Rosenberg, S. (2010). Myeloid-derived suppressor cells: More mechanisms for inhibiting antitumor immunity. *Cancer Immunology, Immunotherapy*, *59*(10), 1593–1600. https://doi.org/10.1007/s00262-010-0855-8

83. Eder, K., & Kalman, B. (2015). The dynamics of interactions among immune and glioblastoma cells. *NeuroMolecular Medicine*, *17*(4), 335–352. https://doi.org/10.1007/s12017-015-8362-x

84. Yang, I., Tihan, T., Han, S. J., Wrensch, M. R., Wiencke, J., Sughrue, M. E., & Parsa, A. T. (2010). Cd8+ T-cell infiltrate in newly diagnosed glioblastoma is associated with long-term survival. *Journal of Clinical Neuroscience*, *17*(11), 1381–1385. https://doi.org/10.1016/j.jocn.2010.03.031

85. Mohme, M., & Neidert, M. C. (2020). Tumor-specific T cell activation in malignant brain tumors. *Frontiers in Immunology*, *11*. https://doi.org/10.3389/fimmu.2020.00205

86. Dranoff, G. (2004). Cytokines in cancer pathogenesis and cancer therapy. *Nature Reviews Cancer*, *4*(1), 11–22. https://doi.org/10.1038/nrc1252

87. Farhood, B., Najafi, M., & Mortezaee, K. (2018). CD8 + cytotoxic T lymphocytes in cancer immunotherapy: A Review. *Journal of Cellular Physiology*, *234*(6), 8509–8521. https://doi.org/10.1002/jcp.27782

88. Joffre, O. P., Segura, E., Savina, A., & Amigorena, S. (2012). Cross-presentation by dendritic cells. *Nature Reviews Immunology*, *12*(8), 557–569. https://doi.org/10.1038/nri3254

89. Woroniecka, K., Chongsathidkiet, P., Rhodin, K., Kemeny, H., Dechant, C., Farber, S. H., Elsamadicy, A. A., Cui, X., Koyama, S., Jackson, C., Hansen, L. J., Johanns, T. M., Sanchez-Perez, L., Chandramohan, V., Yu, Y.-R. A., Bigner, D. D., Giles, A., Healy, P., Dranoff, G., … Fecci, P. E. (2018). T-cell exhaustion signatures vary with tumor type and are severe in glioblastoma. *Clinical Cancer Research*, *24*(17), 4175–4186. https://doi.org/10.1158/1078-0432.ccr-17-1846

90. Koyama, S., Akbay, E. A., Li, Y. Y., Herter-Sprie, G. S., Buczkowski, K. A., Richards, W. G., Gandhi, L., Redig, A. J., Rodig, S. J., Asahina, H., Jones, R. E., Kulkarni, M. M., Kuraguchi, M., Palakurthi, S., Fecci, P. E., Johnson, B. E., Janne, P. A., Engelman, J. A., Gangadharan, S. P., … Hammerman, P. S. (2016). Adaptive resistance to therapeutic PD-1 blockade is associated with upregulation of alternative immune checkpoints. *Nature Communications*, *7*(1). https://doi.org/10.1038/ncomms10501

91. Kadiyala, P., Carney, S. V., Gauss, J. C., Garcia-Fabiani, M. B., Haase, S., Alghamri, M. S., Núñez, F. J., Liu, Y., Yu, M., Taher, A., Nunez, F. M., Li, D., Edwards, M. B., Kleer, C. G., Appelman, H., Sun, Y., Zhao, L., Moon, J. J., Schwendeman, A., … Castro, M. G. (2021). Inhibition of 2-hydroxyglutarate elicits metabolic reprogramming and mutant IDH1 glioma immunity in mice. *Journal of Clinical Investigation*, *131*(4). https://doi.org/10.1172/jci139542

92. Tay, R. E., Richardson, E. K., & Toh, H. C. (2020). Revisiting the role of CD4+ T cells in cancer immunotherapy—new insights into old paradigms. *Cancer Gene Therapy*, *28*(1-2), 5–17. https://doi.org/10.1038/s41417-020-0183-x

93. Ghouzlani, A., Kandoussi, S., Tall, M., Reddy, K. P., Rafii, S., & Badou, A. (2021). Immune checkpoint inhibitors in human glioma microenvironment. *Frontiers in Immunology*, *12*. https://doi.org/10.3389/fimmu.2021.679425

94. Wherry, E. J. (2011). T cell exhaustion. *Nature Immunology*, *12*(6), 492–499. https://doi.org/10.1038/ni.2035

95. Schietinger, A., & Greenberg, P. D. (2014). Tolerance and exhaustion: Defining mechanisms of T cell dysfunction. *Trends in Immunology*, *35*(2), 51–60. https://doi.org/10.1016/j.it.2013.10.001

96. Jiang, W., He, Y., He, W., Wu, G., Zhou, X., Sheng, Q., Zhong, W., Lu, Y., Ding, Y., Lu, Q., Ye, F., & Hua, H. (2021). Exhausted CD8+T cells in the tumor immune microenvironment: New pathways to therapy. *Frontiers in Immunology*, *11*. https://doi.org/10.3389/fimmu.2020.622509

97. Wherry, E. J., & Kurachi, M. (2015). Molecular and cellular insights into T cell exhaustion. *Nature Reviews Immunology*, *15*(8), 486–499. https://doi.org/10.1038/nri3862

98. Petrovas, C., Casazza, J. P., Brenchley, J. M., Price, D. A., Gostick, E., Adams, W. C., Precopio, M. L., Schacker, T., Roederer, M., Douek, D. C., & Koup, R. A. (2006). PD-1 is a regulator of virus-specific CD8+ T cell survival in HIV infection. *Journal of Experimental Medicine*, *203*(10), 2281–2292. https://doi.org/10.1084/jem.20061496

99. Petrovas, C., Price, D. A., Mattapallil, J., Ambrozak, D. R., Geldmacher, C., Cecchinato, V., Vaccari, M., Tryniszewska, E., Gostick, E., Roederer, M., Douek, D. C., Morgan, S. H., Davis, S. J., Franchini, G., & Koup, R. A. (2007). Siv-specific CD8+ T cells express high levels of PD1 and cytokines but have impaired proliferative capacity in acute and chronic SIVMAC251 infection. *Blood*, *110*(3), 928–936. https://doi.org/10.1182/blood-2007-01-069112

100. Blackburn, S. D., Crawford, A., Shin, H., Polley, A., Freeman, G. J., & Wherry, E. J. (2010). Tissue-specific differences in PD-1 and PD-L1 expression during chronic viral infection: Implications for CD8 T-cell exhaustion. *Journal of Virology*, *84*(4), 2078–2089. https://doi.org/10.1128/jvi.01579-09

101. Blackburn, S. D., Shin, H., Freeman, G. J., & Wherry, E. J. (2008). Selective expansion of a subset of exhausted CD8 T cells by αPD-L1 blockade. *Proceedings of the National Academy of Sciences*, *105*(39), 15016–15021. https://doi.org/10.1073/pnas.0801497105

102. Blackburn, S. D., Shin, H., Haining, W. N., Zou, T., Workman, C. J., Polley, A., Betts, M. R., Freeman, G. J., Vignali, D. A., & Wherry, E. J. (2008). Coregulation of CD8+ T cell exhaustion by multiple inhibitory receptors during chronic viral infection. *Nature Immunology*, *10*(1), 29–37. https://doi.org/10.1038/ni.1679

103. Workman, C. J., Cauley, L. S., Kim, I.-J., Blackman, M. A., Woodland, D. L., & Vignali, D. A. (2004). Lymphocyte activation gene-3 (CD223) regulates the size of the expanding T cell population following antigen activation in vivo. *The Journal of Immunology*, *172*(9), 5450–5455. https://doi.org/10.4049/jimmunol.172.9.5450

104. Parry, R. V., Chemnitz, J. M., Frauwirth, K. A., Lanfranco, A. R., Braunstein, I., Kobayashi, S. V., Linsley, P. S., Thompson, C. B., & Riley, J. L. (2005). CTLA-4 and PD-1 receptors inhibit T-cell activation by distinct mechanisms. *Molecular and Cellular Biology*, *25*(21), 9543–9553. https://doi.org/10.1128/mcb.25.21.9543-9553.2005

105. Quigley, M., Pereyra, F., Nilsson, B., Porichis, F., Fonseca, C., Eichbaum, Q., Julg, B., Jesneck, J. L., Brosnahan, K., Imam, S., Russell, K., Toth, I., Piechocka-Trocha, A., Dolfi, D., Angelosanto, J., Crawford, A., Shin, H., Kwon, D. S., Zupkosky, J., … Haining, W. N. (2010). Transcriptional analysis of HIV-specific CD8+ T cells shows that PD-1 inhibits T cell function by upregulating BATF. *Nature Medicine*, *16*(10), 1147–1151. https://doi.org/10.1038/nm.2232

106. Drake, C. G., Jaffee, E., & Pardoll, D. M. (2006). Mechanisms of immune evasion by tumors. *Advances in Immunology*, 51–81. https://doi.org/10.1016/s0065-2776(06)90002-9

107. Armand, P. (2015). Immune checkpoint blockade in hematologic malignancies. *Blood*, *125*(22), 3393–3400. https://doi.org/10.1182/blood-2015-02-567453

108. Sharma, P., & Allison, J. P. (2020). Dissecting the mechanisms of immune checkpoint therapy. *Nature Reviews Immunology*, *20*(2), 75–76. https://doi.org/10.1038/s41577-020-0275-8

109. Chraa, D., Naim, A., Olive, D., & Badou, A. (2018). T lymphocyte subsets in Cancer immunity: Friends or foes. *Journal of Leukocyte Biology*, *105*(2), 243–255. https://doi.org/10.1002/jlb.mr0318-097r

110. Goswami, S., Walle, T., Cornish, A. E., Basu, S., Anandhan, S., Fernandez, I., Vence, L., Blando, J., Zhao, H., Yadav, S. S., Ott, M., Kong, L. Y., Heimberger, A. B., de Groot, J., Sepesi, B., Overman, M., Kopetz, S., Allison, J. P., Pe'er, D., & Sharma, P. (2019). Immune profiling of human tumors identifies CD73 as a combinatorial target in glioblastoma. *Nature Medicine*, *26*(1), 39–46. https://doi.org/10.1038/s41591-019-0694-xj